The net charge of the K-loop regulates KIF1A superprocessivity by enhancing microtubule affinity in the one-head-bound state

Taylor M. Zaniewski and William O. Hancock*

Departments of Chemistry and Biomedical Engineering, Pennsylvania State University, University Park, Pennsylvania, USA

* Corresponding Author
William O. Hancock
122 CBEB
University Park, PA 16802
(814) 863-0492
woh1@psu.edu

Acknowledgements:

The authors thank Dr. Kristen Verhey for helpful discussions that resolved differences between the current results and previously published KIF1A data. The authors thank the Hancock lab group members for their helpful discussions, with particular thanks to Adheshwari Ramesh and Samira Bell for their help making the plasmids used in this study.

Abstract:

KIF1A is an essential neuronal transport motor protein in the kinesin-3 family, known for its superprocessive motility. We determined that superprocessivity of KIF1A dimers originates from a unique structural domain, the lysine rich insertion in loop-12 termed the 'K-Loop', which enhances electrostatic interactions between the motor and the microtubule. In 80 mM PIPES buffer, replacing the native loop-12 of KIF1A with that of kinesin-1, resulted in a 6-fold decrease in run length, and adding additional positive charge to loop-12 enhanced the run length. Interestingly, swapping the KIF1A loop-12 into kinesin-1 did not enhance its run length, consistent with the two motor families using different mechanochemical tuning to achieve persistent

transport. To investigate the mechanism by which the KIF1A K-loop enhances processivity, we used microtubule pelleting and single-molecule dwell times assays in ATP and ADP. First, the microtubule affinity was similar in ATP and in ADP, consistent with the motor spending the majority of its cycle in a weakly-bound state. Second, the microtubule affinity and single-molecule dwell time in ADP were 6-fold lower in the loop-swap mutant compared to wild type. Thus, the positive charge in loop-12 of KIF1A enhances the run length by stabilizing the motor binding in its vulnerable one-head-bound state. Finally, through a series of mutants with varying positive charge in the K-loop, we found that the KIF1A processivity is linearly dependent on the charge of loop-12.

Introduction

KIF1A is a fast and superprocessive neuronal transport motor protein in the kinesin-3 family that is responsible for the delivery of synaptic vesicle precursors from the soma to the distal end of the axon, among other tasks.[1–5] Genetic mutations lead to KIF1A Associated Neurological Disorders (KAND), rare and often misdiagnosed afflictions.[5–14] The category of KAND is vast, with 113 variants that have been identified in humans so far, making therapeutic attempts difficult.[14] Therefore, approaching treatments more systematically requires a deeper understanding of the fundamental mechanochemical mechanism of KIF1A.

A recent biochemical dissection of the KIF1A chemomechanical cycle concluded that: i) both ATP binding and hydrolysis are required to trigger tethered-head binding, ii) rear head detachment is fast and may contribute to the fast stepping rate, and iii) the motor spends the majority of its stepping cycle in a post-hydrolysis, one-head-bound (1HB) state.[15] This ability to remain associated with the microtubule in a "weakly-bound" state enhances the motor processivity by ensuring that the motor remains bound to the microtubule sufficiently long for the tethered head to complete its step and bind to the next site.[16–18] This property of remaining in a vulnerable one-head-bound state also provides an explanation for the propensity of KIF1A to detach readily under load.[19–22] A recent optical trapping study that used a three-bead geometry to minimize forces oriented perpendicular to the microtubule concluded that under load KIF1A is able to sustain loads by rapidly rebinding to the microtubule following disengagement.[20] Because KIF1A does not achieve high microtubule affinity by maximizing the duration spent in a strong binding two-head-

bound state, we proposed that the source of its processivity is a combination of a relatively slow detachment rate from the post-hydrolysis 1HB state and faster tethered-head attachment rate compared to kinesin-1 and -2.[15] The goal of the current study was to define the structural elements of KIF1A that underlie this kinetic tuning.

The kinesin-3 family is known for a unique structural domain called the K-Loop. This domain is a stretch of Loop-12 in which KIF1A contains six lysine residues and kinesin-1 and -2 only have one lysine.[23] In early work it was determined that the electrostatic interaction of the K-Loop with the microtubule facilitates diffusive motion, leading to monomeric motility of KIF1A.[23–25] The enhanced positive charge of KIF1A in this region is thought to interact with the glutamate rich C-terminal tail of tubulin, termed the 'E-hook'.[26,27] However, because these domains are disordered, and their structures and interactions not resolved by X-ray crystallography or CryoEM,[26,28,29] biochemical and single-molecule investigations are vital for understanding this interaction.

In the literature, there are conflicting reports regarding the role of the K-loop in KIFA superprocessivity, with some studies indicating that the K-loop is responsible for KIF1A superprocessivity,[27,30] and others suggesting that the K-loop plays no role in the processivity of KIF1A and only increases its microtubule on-rate.[31] This lack of consensus in the field has led to considerable confusion regarding the role of the K-loop in long distance intracellular transport. In the present study, we used single-molecule microscopy and stopped-flow biochemical experiments to clarify the role of loop-12 in KIF1A motility. By using a series of mutations, buffers, and experimental approaches, we determined that at near physiological ionic strength the K-loop enhances the processivity of KIF1A by strengthening the microtubule affinity of a vulnerable one-head-bound state in the KIF1A chemomechanical cycle. Additionally, this functionality cannot be transferred to kinesin-1, highlighting how different motor families use distinct biochemical tuning to achieve fast and processive motility.

Results

Influence of the neck-coil and coiled-coil domains on KIF1A motility

To understand how different structural elements of KIF1A contribute to its motility and to reconcile conflicting results in the literature, we designed constitutively active constructs of KIF1A that included different distal coiled-coil domains to ensure stable KIF1A dimers and included or excluded the native neck-coil domain of KIF1A. All of the KIF1A constructs are based on a truncated and constitutively active KIF1A dimer that has been used in a number of published studies.[15,27,31,32] The 'neck-coil', defined as residues 369-393 of *Rattus norvegicus* KIF1A, is a short coiled-coil domain that is immediately distal to the disordered neck linker domain and is involved in dimerization of the two motor domains.[33,34] Based on other members of the kinesin-3 family, it is thought that in full-length KIF1A, coiled-coil 1 folds back on the neck-coil and forms an antiparallel coiled-coil that separates the two heads and inhibits motor activity.[32,33] It was shown previously that the neck-coil alone is insufficient to stably dimerize KIF1A,[32–34] and that this could be rectified by adding a leucine zipper (LZ) downstream of the neck-coil.[19,27,32] A second approach to dimerizing diverse kinesins has been to fuse the motor and neck linker domains to the coiled-coil domain of *D. melanogaster* kinesin-1.[15,17,35–37]

To directly compare how these different dimerization strategies affect KIF1A motility, we designed three dimeric, GFP-tagged *Rattus norvegicus* KIF1A constructs, as follows. The first construct consisted of KIF1A residues 1-393 followed by a leucine zipper domain and GFP, which we refer to as 1A-LZ (Fig. 1A). This construct matches those used in a number of published studies, albeit with different C-terminal tags.[19,27,30,32] We made two other constructs that achieved stable dimerization through the *Drosophila melanogaster* kinesin heavy chain (KHC) neck-coil and coiled-coil 1 domains (345-560). The first construct, which includes the KIF1A neck-coil, fused KIF1A(1-393) to residues 345-560 of KHC and a C-terminal GFP, which we refer to as $1A_{393}$ (Fig. 1A-B). The second construct, which does not include the KIF1A neck-coil and was used in a previous study,[15] fused KIF1A(1-368) to residues 345-560 of KHC and a C-terminal GFP. We refer to this as $1A_{368}$ (Fig. 1A).

To reconcile the behavior of disparate constructs in the literature, the first question we addressed was whether the dimerization strategy affected the KIF1A run length in 80 mM PIPES (BRB80) buffer. We found that 1A-LZ had a 2-fold longer run length than $1A_{393}$ (6.1 ± 0.1 and 3.0 ± 0.02 μm, respectively; Fig. 1C with raw data in Fig. S1). We propose that this difference in processivity is due to the differential charge in the coiled-coil domains rather than differences in interhead coordination between the two constructs. The net charge of coil-1 of KIF1A, which these dimerization domains replace, is -6; the net charge of the kinesin-1 neck-coil (345-405) is -3; and the net charge of the leucine zipper is neutral (Fig. S2). It was shown previously that adding positive charge to the kinesin-1 coiled-coil enhances its run length and adding negative charge diminishes its run length.[38] Thus, we interpret the longer run length of 1A-LZ to be due to enhanced interaction between the coiled-coil domain and the negatively charged C-terminus of tubulin. One prediction of this hypothesis is that the motor off-rate in ADP, which induces a weak-binding state that doesn't involve coordinated activities of the two heads, should be similarly affected by the electrostatic interactions between the coiled-coil and the microtubule. To probe this question, we used TIRF microscopy to measure the microtubule dwell time of the two constructs in saturating ADP. Consistent with the run length differences, $1A_{393}$-LZ had a ~3-fold longer dwell time than $1A_{393}$ (Fig. 1F). Thus, because the negative net charge of the Kin1 neck-coil sequence better matches the native KIF1A, and because this domain has been used in a body of our previous work, we focused our efforts on the $1A_{393}$ construct.

Because the KIF1A neck-coil domain has been shown to be insufficient to form a stable dimer on its own,[32] it is possible that even in constructs dimerized by fusing a distal coiled-coil domain, the neck-coil does not form a stable connection between the two motor domains. This 'breathing' of the neck-coil could affect the interhead coordination necessary for processivity, consistent with previous work that showed extending the length of the kinesin neck linker, which connects each motor domain to their shared neck-coil, reduced motor run lengths.[34,39–41] To test whether the KIF1A neck-coil plays a role beyond dimerization, we used TIRF microscopy in BRB80 buffer to compare the run length of $1A_{393}$, which includes the neck-coil, to $1A_{368}$, which lacks the neck-coil (Fig. 1A). The two constructs had similar run lengths, indicating that the sequence and stability of the KIF1A neck-coil has no effect on its processivity (Fig. 1B, D). Consistent with the run lengths, the microtubule dwell times of the two motors in 2 mM ADP, which probes the affinity in the

154 weak-binding state, were also similar (Fig. 1G). We hypothesized that if there is any reversible
155 dimerization in the KIF1A neck-coil, then it may have a stronger effect on kinesin-1, which has a
156 shorter neck linker domain and thus a stiffer connection between the two heads than KIF1A.[17,40–
157 43] To test this, we used *Drosophila* kinesin-1 truncated at residue 557 and fused to GFP, which has
158 been used in numerous previous studies, and is referred to as Kin1 here.[15,17,35,36] The KIF1A neck-
159 coil domain (KIF1A 369-393) was inserted just upstream of Ala_{345} at the start of the neck-coil of
160 Kin1 to generate $K1_{1Anc}$ (Fig. 1A).[44] In single-molecule assays, the Kin1 run length was 0.8 ± 0.02
161 μm/s (Fig. 1E), which is consistent with previous work and is four-fold shorter than KIF1A (Fig.
162 1C).[17,35,36] $K1_{1Anc}$ had a ~2-fold shorter run length than Kin1 (0.4 ± 0.002 μm; Fig. 1D) and also
163 had a slightly slower velocity (0.5 ± 0.2 μm/s versus 0.7 ± 0.2 μm/s; Fig. 1E). It is unlikely that
164 the shorter run length of $K1_{1Anc}$ results from differences in positive charge in the neck-coil domain,
165 because both the kinesin-1 and KIF1A neck-coil domains are negatively charged (-3 for Kin1 and
166 -2 for KIF1A; Fig. S2). Instead, the shorter run length of $K1_{1Anc}$ is consistent with the KIF1A neck-
167 coil dimerizing only weakly and acting as an extended neck linker in kinesin-1, loosening the
168 connection between the two motor domains and reducing its performance.[17,40–42] In light of this, it
169 is surprising that replacing the KIF1A neck-coil with the more stable kinesin-1 neck-coil does not
170 enhance the KIF1A run length. However, the native neck linker domain of KIF1A is longer than
171 that of kinesin-1,[43] and so one possibility is that stabilizing the KIF1A neck region by adding the
172 kinesin-1 coiled-coil is not sufficient to establish a tight connection between the two heads. It
173 follows that the superprocessivity of KIF1A does not result from tight mechanical connection
174 between the heads to achieve coordinated stepping, but rather from other aspects of the motor's
175 chemomechanics.
176
177 **Influence of ionic strength on KIF1A motility**
178 To better understand the role of electrostatic interactions in KIF1A motility and to reconcile diverse
179 studies across the literature, we investigated the effect of buffer ionic strength on KIF1A motility.
180 We chose two buffers commonly used in the literature: BRB80, which contains 80 mM PIPES and
181 has a 173 mM ionic strength, and BRB12, which contains 12 mM PIPES and has a 26 mM ionic
182 strength (both buffers also include 1 mM $MgCl_2$, 1 mM EGTA, pH 6.9). Although much of the
183 published work on KIF1A was performed in BRB12,[19,27,31,32] the ionic strength of BRB80 (173
184 mM) is closer to the ~200 mM ionic strength estimated in cells.[45] The low ionic strength of BRB12

185 is expected to maximize electrostatic interactions between motors and microtubules; for instance,
186 the Debye length in BRB80 is 0.7 nm in BRB80 and 2 nm in BRB12.[46]
187
188 Consistent with enhanced electrostatic interactions, we found that $1A_{393}$ had a nearly 5-fold longer
189 run length in BRB12 compared to BRB80 (14.3 ± 0.4 μm versus 3.0 ± 0.02; Fig. 1C). Additionally,
190 we observed increased pausing behavior at low ionic strength, as reported previously.[27] Thus, we
191 quantified the segmented velocity (Fig. 1D) and found that the velocity decreased from 1.5 μm/s
192 in BRB80 to 1.1 μm/s in BRB12. The longer run length and slower velocity correspond to a
193 substantially higher affinity of KIF1A for microtubules in BRB12 buffer. To compare the
194 microtubule affinity of KIF1A in its weak-binding ADP state in these different buffers, we
195 measured the microtubule dwell time in 2 mM ADP and found that the dwell time in BRB12 was
196 10-fold longer than in BRB80 (Fig. 1F). Thus, the enhanced run length of KIF1A in BRB12 can
197 be explained by the reduced charge shielding at lower ionic strength enhancing the electrostatic
198 interaction between the microtubule and KIF1A in the weakly-bound ADP state. Because these
199 enhanced electrostatic interactions in BRB12 may mask other aspects of KIF1A
200 mechanochemistry, we focused our efforts on characterizing KIF1A in BRB80, which is closer to
201 physiological ionic strength.

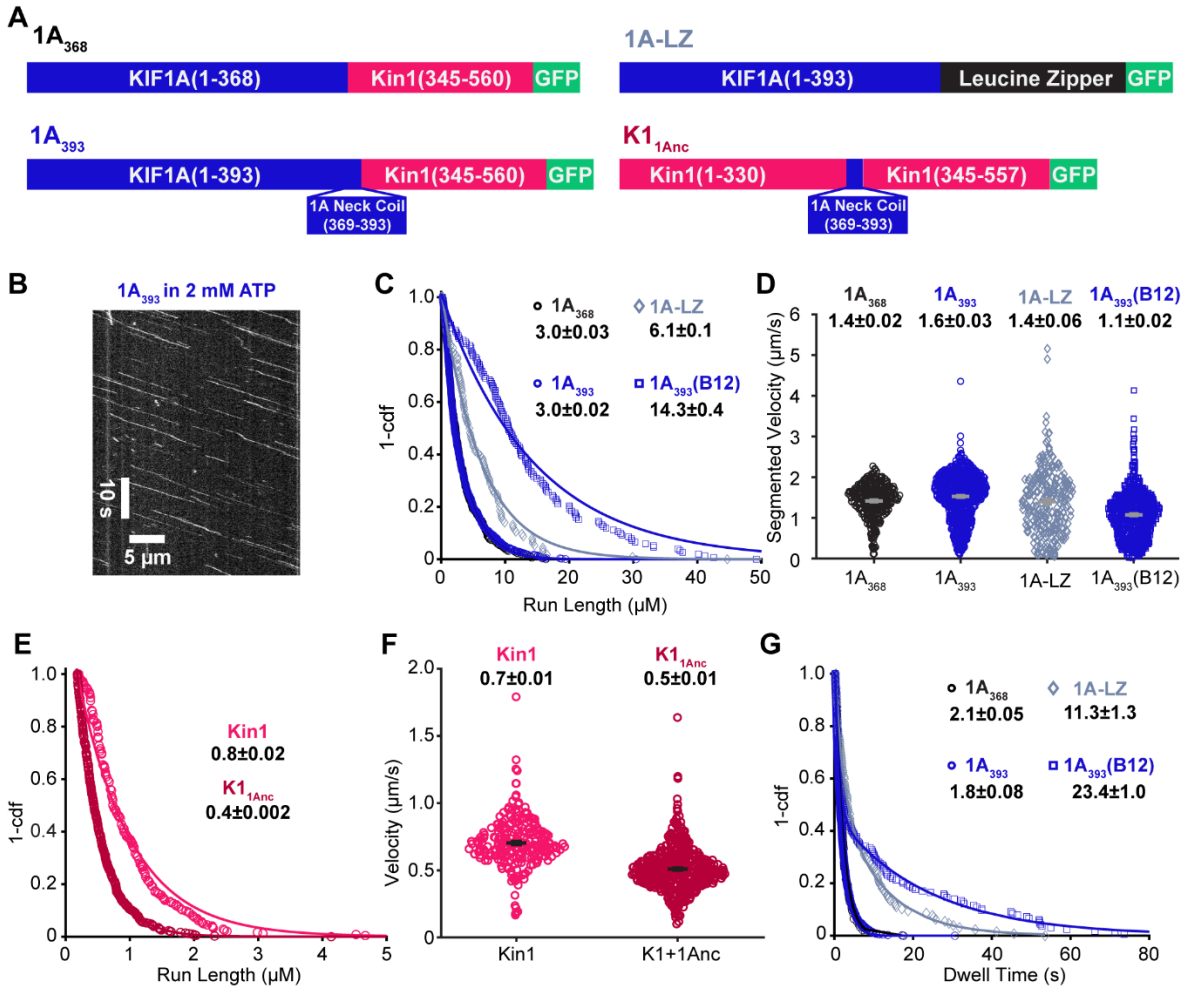

Figure 1: **Dimerization domain and buffer ionic strength impact KIF1A motility**

A, Diagrams of the protein constructs used in this study. KIF1A refers to *Rattus norvegicus* KIF1A; Kin1 refers to *Drosophila melanogaster* kinesin heavy chain. **B,** Example kymograph of $1A_{393}$ in 2 mM ATP and BRB80. Scale bars are 10 sec and 5 µm. **C,** Run length distribution of $1A_{368}$ (black circles), $1A_{393}$ (blue circles), $1A_{393}$-LZ (navy diamonds), and $1A_{393}$ in BRB12 (blue squares). Single exponential fits give run lengths of 3.0 ± 0.03, 3.0 ± 0.02, 6.1 ± 0.1, and 14.3 ± 0.4 µm, respectively (fit ± 95% confidence interval). **D,** Velocity distribution of $1A_{368}$ (black circles), $1A_{393}$ (blue circles), $1A_{393}$-LZ (navy diamonds), and $1A_{393}$ in BRB12 (blue squares). Average segmented velocities are 1.4 ± 0.02, 1.6 ± 0.03, 1.4 ± 0.06, 1.1 ± 0.02 µm/s, respectively (mean ± SEM). **E,** Run length distribution of Kin1 (pink) and $K1_{1Anc}$ (red). Single exponential fits give run lengths of 0.8 ± 0.02, and 0.4 ± 0.002 µm, respectively (fit ± 95% confidence interval). **F,** Velocity distribution of Kin1 (pink) and $K1_{1Anc}$ (red). Average velocities are 0.7 ± 0.2 and 0.5 ± 0.2 µm/s, respectively (mean ± SD). **G,** Dwell time distributions in 2 mM ADP. Single

216 exponential fits to $1A_{368}$ (black circles) and $1A_{393}$ (blue circles) give dwell times of 2.1 ± 0.05 and
217 1.8 ± 0.08 s, respectively. $1A_{393}$-LZ (navy diamonds) and $1A_{393}$ in BRB12 (blue squares) were fit
218 with biexponentials. $1A_{393}$-LZ had dwell times of 2.0 ± 0.3 and 11.3 ± 1.3 s, and $1A_{393}$ in BRB12
219 had dwell times of 1.1 ± 0.04 and 23.4 ± 1.0 s; the longer duration for each is presented in the
220 figure.
221

222 **K-loop regulates the run length of KIF1A but not Kin-1**

223 Earlier studies of KIF1A monomers found that the positively charged Loop-12 of KIF1A enhances
224 its microtubule affinity,[23] however subsequent studies of KIF1A dimers have reported Loop-12
225 does not contribute to superprocessivity.[31] To test whether the K-Loop is responsible for the
226 superprocessivity of our KIF1A construct in BRB80 buffer, we examined the properties of a
227 'swap' construct, in which the native loop-12 of KIF1A is removed and replaced with the kinesin-
228 1 loop-12, KIF1A(1-393)-Kin1Loop12-K560-GFP (referred to as 1A-K1L12; Fig. 2A).[23,31]
229 Swapping out the KIF1A Loop-12 caused a 6-fold decrease in the run length and a slight decrease
230 in velocity, consistent with Loop-12 being the determinant of KIF1A superprocessivity (Fig. 2 B-
231 C and Fig. S3).
232

233 If Loop-12 is enhancing KIF1A processivity by enhancing electrostatic interactions with the
234 microtubule, then in principle swapping it into kinesin-1 should enhance the run length, and
235 previous work found this to be the case in low ionic strength buffer.[31] To test this question in
236 BRB80 buffer where physiological charge shielding is expected, we made a 'reverse swap' mutant,
237 in which the KIF1A loop-12 was inserted into kinesin-1, replacing the native loop-12 (referred to
238 as K1-1AL12; Fig. 2A). Surprisingly, inserting the positively charged KIF1A K-loop into Kin-1
239 did not impact the velocity or run length (Fig. 2E-F; see Fig. S3 for representative kymographs).
240 Thus, due to differences in the microtubule binding interface and/or kinetic tuning of kinesin-1,
241 adding the positively charged K-loop into kinesin-1 does not enhance its processivity in near
242 physiological ionic strength buffer.

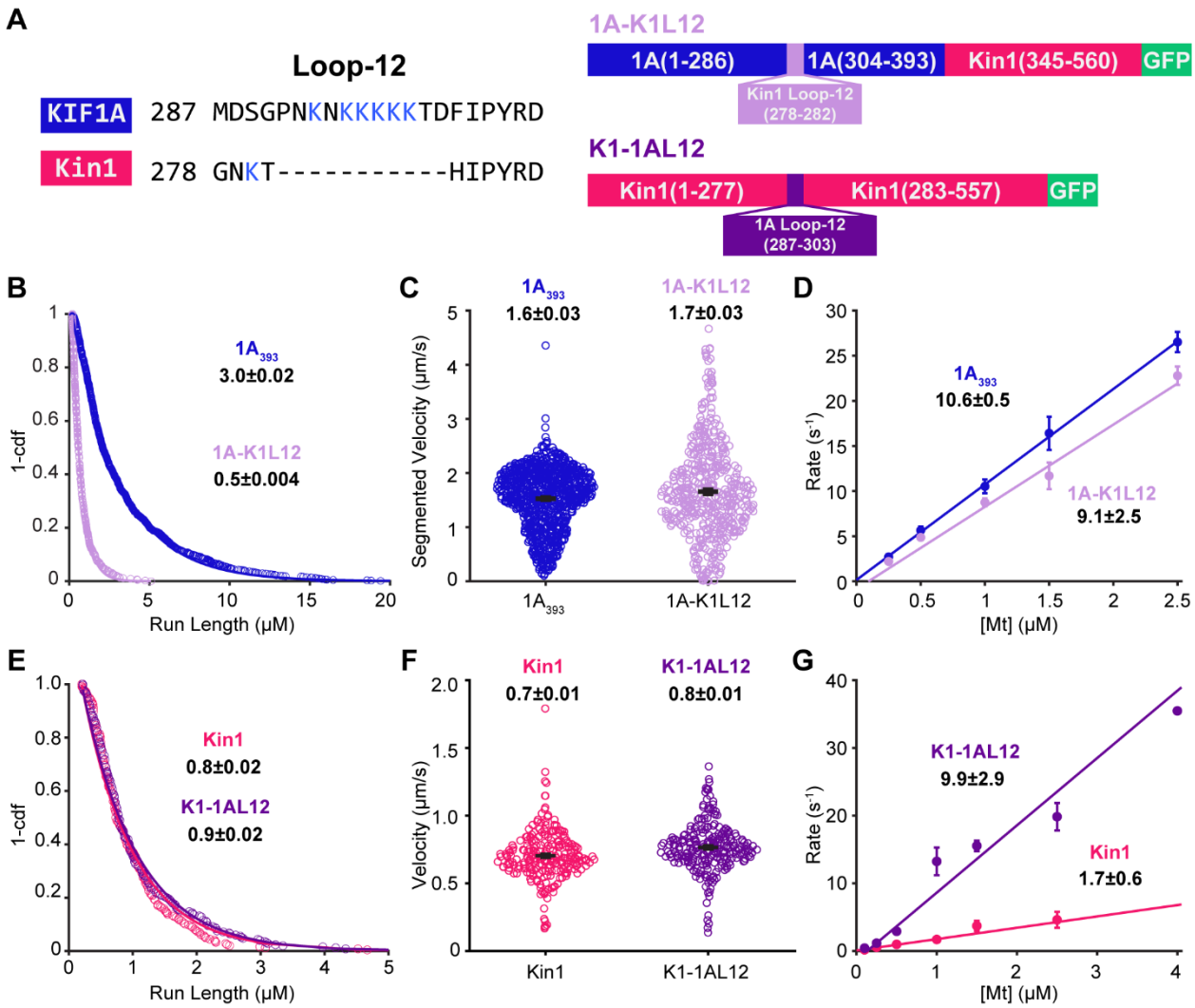

Figure 2: **K-Loop is the source of KIF1A superprocessivity**

A, Diagrams of the loop swap constructs. **B,** Run length distribution of $1A_{393}$ (blue circles) and 1A-K1L12 (light purple circles) in BRB80 and 2 mM ATP. Values are single exponential fit ± 95% confidence interval. **C,** Velocity distribution of $1A_{393}$ (blue circles) and 1A-K1L12 (light purple circles) in BRB80 and 2 mM ATP. Average segmented velocities values are mean ± SEM. P<0.0001 **D,** Bimolecular on-rates of $1A_{393}$ (blue circles) and 1A-K1L12 (light purple circles), using motors lacking coiled-coil 1 and GFP (see Methods). Linear fits give k_{on}^{Mt} (fit ± 95% confidence interval). Points are mean ± SEM. **E,** Run length distribution of Kin1 (pink circles) and K1-1AL12 (dark purple circles) in BRB80 and 2 mM ATP. Values are single exponential fit ± 95% confidence interval. **F,** Velocity distribution of Kin1 (pink circles) and K1-1AL12 (dark purple circles) in BRB80 and 2 mM ATP. Values are mean ± SEM. P<0.0001 **G,** Bimolecular on-

255 rates of Kin1 (pink circles) and K1-1AL12 (dark purple circles). Linear fits give k_{on}^{Mt} (fit ± 95%
256 confidence interval). Points are mean ± SEM.
257
258 To further investigate how positive charge in loop-12 differentially affects KIF1A and kinesin-1,
259 we compared the effects of the loop swap on the microtubule on-rate of the two motors. Using
260 stopped-flow, the bimolecular on-rate (k_{on}^{Mt}) was measured by incubating the motors with
261 fluorescently labeled mant-ADP in BRB80 and flushing the solution against varying
262 concentrations of taxol-stabilized microtubules in 2 mM ADP. Upon mixing, the motors bind to
263 the microtubule and release the mant-ADP, which results in a fall in fluorescence. Because at low
264 microtubule concentrations mant-ADP release is rate limited by microtubule binding, a linear fit
265 of the rates to the microtubule concentration yields the bimolecular on-rate.[15,42,47,48] Notably,
266 swapping the K-loop out of KIF1A had little effect on the bimolecular on-rate of KIF1A,
267 contrasting with its effect on the run length (Fig. 2D). However, swapping the KIF1A loop-12 into
268 kinesin-1 caused a 5-fold increase in the on-rate (Fig. 2G).
269

270 **Positive charge in the KIF1A K-loop enhances processivity by decreasing the rate of**
271 **detachment from a vulnerable 1HB state**

272 To investigate the mechanism by which the K-Loop enhances KIF1A processivity, we quantified
273 key rate constants in the KIF1A chemomechanical cycle that determine motor run length. Previous
274 work established that kinesin processivity is determined by a kinetic race as the motor takes a
275 forward step, as follows.[17,18] Following ATP hydrolysis, kinesin is in a vulnerable one-head-bound
276 state that can resolve either by the tethered head completing a forward step by binding to the next
277 tubulin binding site and transitioning to a tight binding state, or by the motor dissociating from the
278 microtubule and terminating the run (Fig. 3A).[15,17] Thus, in principle the K-loop could enhance
279 KIF1A processivity by some combination of increasing the on-rate that the tethered head binds to
280 its next binding site (k_{on}^{TH}) and decreasing the rate that the bound head detaches from the
281 microtubule (k_{detach}).
282
283 To test whether the K-loop affects the detachment rate of KIF1A from its weak-binding state, we
284 used an affinity assay in conjunction with a microtubule on-rate measurement. The dissociation

285 constant is defined as $K_D = \frac{k_{detach}}{k_{on}^{Mt}}$; thus, by measuring both K_D and k_{on}^{Mt} for each motor, we can
286 calculate k_{detach}. To estimate the K_D of $1A_{393}$ and 1A-K1L12, we carried out a microtubule pelleting
287 assay in 2 mM ADP to mimic the weak-binding post-hydrolysis state. In this assay, varying
288 concentrations of microtubules are mixed together with a constant concentration of motors, the
289 mixture is pelleted, and the GFP fluorescence is used to determine the fraction of motors bound to
290 the microtubule at each [Mt].[42] As shown in Fig. 3B, swapping out Loop-12 of KIF1A reduced the
291 microtubule affinity in ADP by four-fold, with $K_D = 1.3 \pm 0.8$ μM for $1A_{393}$, and $K_D = 5.1 \pm 4.3$
292 μM for 1A-K1L12. To relate these affinities to the affinity of the motor when it is processively
293 walking along the microtubule, we repeated these pelleting assays in ATP. For both constructs,
294 their K_D in ATP was similar to that in ADP (for $1A_{393}$, $K_D = 1.7 \pm 1.0$ μM in ATP and for 1A-
295 K1L12, $K_D = 7.2 \pm 5.1$ μM in ATP; Fig. 3B), consistent with both motors spending most of their
296 hydrolysis cycle in a weakly-bound ADP-like state, in agreement with previous work.[15] To
297 calculate the detachment rate from the weak-binding state, we used the K_D in ADP together with
298 the k_{on}^{Mt} results from Fig. 2D, which were 10.6 ± 0.5 μM^{-1} s^{-1} for $1A_{393}$ and 9.1 ± 2.5 μM^{-1} s^{-1} for
299 1A-K1L12. From these values, we calculated k_{detach} in ADP to be 18 ± 11 s^{-1} for $1A_{393}$ and $66 \pm$
300 50 s^{-1} for 1A-K1L12, matching the 4-fold difference in the run lengths in Fig. 2B.
301
302 To more directly test whether the K-loop slows dissociation of KIF1A from the microtubule in the
303 weakly-bound post-hydrolysis state, we used single-molecule TIRF microscopy to measure the
304 dwell time of landing events in 2 mM ADP. For $1A_{393}$, the dwell time distribution was well fit by
305 a single-exponential with a time constant of 1.8 ± 0.08 s (Fig. 1F), corresponding to an off-rate of
306 0.56 ± 0.02 s^{-1}. When we repeated the experiment for 1A-K1L12, the kymographs showed a
307 population of very transient events along with a population of longer duration events (Fig. S3).
308 The dwell time distribution was well fit to a double exponential with a fast population of $0.03 \pm$
309 0.01 s ($k_{off} = 33$ s^{-1}) that constituted ~40% of the events, and a slow population of 0.3 ± 0.03 s (k_{off}
310 $= 3.3$ s^{-1}) that constituted the other ~60 % of the events (Fig. 3C). Relative to the $1A_{393}$ dwell time
311 of 1.8 s, these 1A-K1L12 dwell times correspond to a 60- and 6-fold faster off-rate when the K-
312 loop of KIF1A is swapped out. Thus, both the microtubule pelleting assay and the single-molecule
313 dwell time assay find that the apparent off-rate of KIF1A in the weakly-bound ADP state is
314 increased when the K-loop is replaced by the equivalent sequence from kinesin-1.

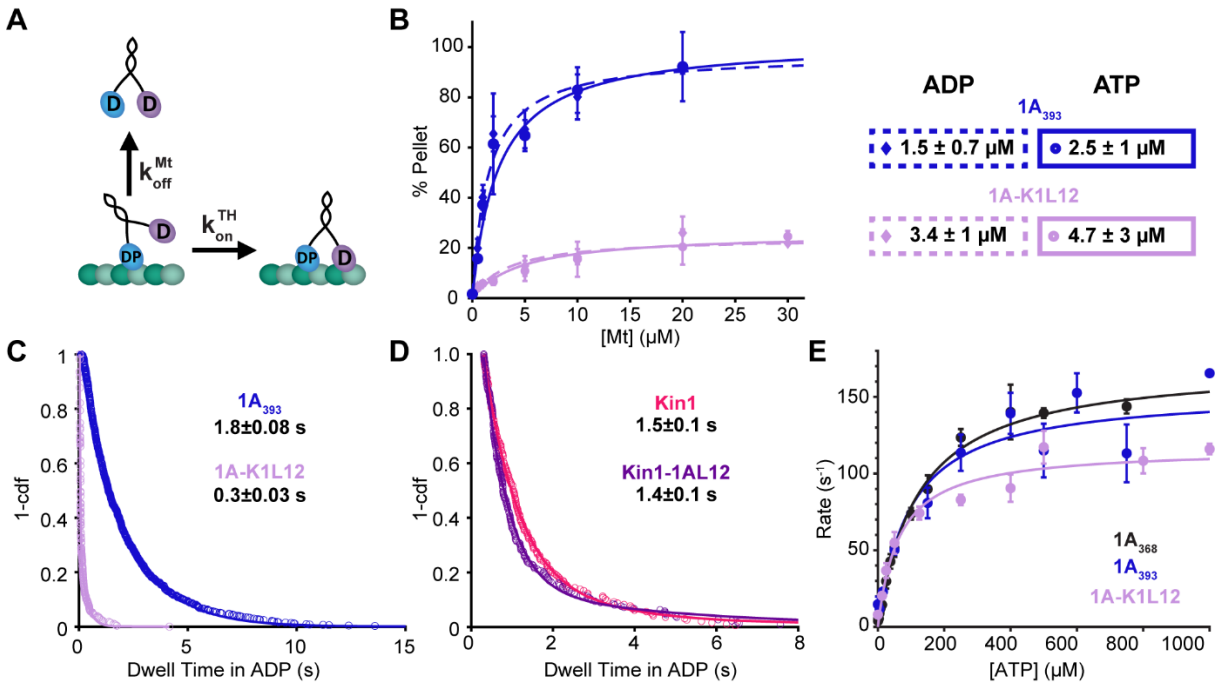

Figure 3: **K-Loop regulates KIF1A superprocessivity via detachment rate in the kinetic race** **A,** Diagram of transitions involved in the Kinetic Race, the tethered-head attachment rate k_{on}^{TH} and the microtubule detachment rate k_{detach}. D, ADP; DP, ADP+Pi. **B,** Microtubule pelleting assay of $1A_{393}$ and 1A-K1L12 in 2 mM ADP or ATP and BRB80. Plot is the percent of GFP-labelled motors in the microtubule pellet after centrifugation as a function of microtubule concentration. To account for any inactive motors, data are normalized to the concentration of motors bound in 1 mM AMPPNP, which induces a strongly-bound state of the motor. Fits with a Langmuir binding isotherm give the K_D and maximal binding fraction for each condition. $1A_{393}$ gives a V_{max} of 97± 10 % and 102 ± 20 % in ADP and ATP, respectively. Despite the normalization to percent binding in AMPPNP, 1A-K1L12 does not reach full binding in this microtubule range with a V_{max} of 24 ± 3 % and 26 ± 7 % in ADP and ATP, respectively. This could be because the K_D is actually around 30 μM or there is only ~50% maximal binding in ADP and ATP. Values are fit ± 95% CI and error bars are mean ± relative error. **C,** Dwell time distribution of 1A-K1L12 (light purple circles) in 2 mM ADP and BRB80. Biexponential fit gives dwell times of 0.03 ± 0.01 s and 0.3 ± 0.03 s (fit ± 95% confidence interval) with equal weights for the fast and slow populations. Data were collected at 50 frames per second. **D,** Dwell time distribution of Kin1 (pink circles) and K1-1AL12 (dark purple circles) in 2 mM ADP and BRB80. Values are single exponential fit ± 95% confidence interval. **E,** ATP-triggered Half-Site Release assay of $1A_{368}$ (black circles), $1A_{393}$ (blue circles),

334 and 1A-K1L12 (light purple circles). Plot is the observed rate as a function of ATP concentration,
335 and fitting with Michaelis-Menten equation give K_M and k_{max} values for each condition. For $1A_{368}$
336 (black circles), $1A_{393}$ (blue circles), and 1A-K1L12 (light purple circles), k_{max} were 172 ± 10, 154
337 ± 30, and 116 ± 13 s^{-1}, respectively; K_M were 119 ± 20, 96 ± 53, and 64 ± 28 μM, respectively (fit
338 ± 95% confidence interval).
339
340 As described by the kinetic race shown in Fig. 3A, it is also possible that the K-loop contributes
341 to KIF1A processivity by enhancing the rate that the tethered head attaches to the microtubule
342 during a forward step. To test this possibility, we carried out an ATP-triggered Half-Site Release
343 assay, as follows (Fig. 3E).[49,50] First, we incubated the motors with mant-ADP and microtubules
344 to establish a complex of motors bound to the microtubule in a one-head-bound state, with mant-
345 ADP trapped in the tethered-head. Then, we flushed this solution against varying concentrations
346 of unlabeled ATP to initiate the binding of the tethered head and subsequent mant-ADP release.
347 We next fit the fluorescent delay from the release of mant-ADP with an exponential function at
348 each ATP concentration, plotted the observed rates versus the corresponding [ATP], and fit the
349 data to a Michaelis-Menten curve. The observed rate constant at saturating ATP concentrations,
350 k_{max}, represents ATP hydrolysis, tethered head binding, and the subsequent release of mant-ADP.
351 Because hydrolysis and mant-ADP are thought to be fast,[15] k_{max} serves as a proxy for the tethered
352 head binding rate. The k_{max} for our $1A_{393}$ construct (154 ± 30 s^{-1}; fit ± 95% confidence interval)
353 was similar to $1A_{368}$ (172 ± 10 s^{-1}), indicating that the neck-coil does not alter the tethered head
354 on-rate. For 1A-K1L12, k_{max} decreased slightly to 116 ± 13 s^{-1}, indicating that, in addition to
355 slowing the microtubule off-rate, the K-loop may enhance KIF1A superprocessivity by increasing
356 the tethered head on-rate, k_{on}^{TH}. However, a caveat of this conclusion is that because the tethered-
357 head attachment is thought to be the rate limiting step of the KIF1A chemomechanical cycle,[15] a
358 decrease in this rate should also decrease the overall motor velocity. Instead, the velocity for 1A-
359 K1L12 was 20% faster than the $1A_{393}$ (Fig. 2C). Additionally, the calculated k_{on}^{TH} for 1A-K1L12
360 of 116 ± 13 s^{-1} is slower than the overall stepping rate of 212 s^{-1} (calculated as 1.7 μm/s velocity
361 ÷ 8 per step). Thus, the question of whether the K-loop enhances the tethered-head on-rate is
362 inconclusive from this experiment.
363

364 As a second strategy for estimating the tethered head attachment rate, we calculated it based on
365 the observed run length in ATP and the measured detachment rate in ADP, as follows. From the
366 kinetic race shown in Fig. 3A,[17] the probability of detaching during each cycle is:

$$p_{detach} = \frac{k_{detach}^{ADP}}{k_{on}^{TH} + k_{detach}^{ADP}} \approx \frac{k_{detach}^{ADP}}{k_{on}^{TH}} \qquad \text{Eq. 1}$$

367 The number of steps a motor takes before dissociating can be estimated as the inverse of the
368 detachment probability:

$$RL_{steps} = \frac{1}{p_{detach}} \approx \frac{k_{on}^{TH}}{k_{detach}^{ADP}} \qquad \text{Eq. 2}$$

369 Thus, the tethered head attachment rate can be estimated by multiplying the measured detachment
370 rate in ADP by the measured run length in ATP:

$$k_{on}^{TH} = k_{detach}^{ADP} * RL_{steps} \qquad \text{Eq. 3}$$

371 Table 1 shows the off-rates in ADP calculated from measured dwell times in Fig. 3 C and D, along
372 with the run lengths calculated in number of steps from Fig. 2 B and E, and the resulting calculated
373 tethered head attachment rate. The first result is that the calculated tethered head on-rates are
374 roughly three-fold faster for KIF1A than kinesin-1, consistent with the faster stepping rate of
375 KIF1A. The key result from this analysis is that for KIF1A, swapping out the K-loop has no effect
376 on the calculated tethered-head on-rate. In summary, the K-loop contributes to the
377 superprocessivity of KIF1A by slowing the off-rate of the motor from the vulnerable 1HB state,
378 and the K-loop does not modulate the processivity of KIF1A by enhancing the tethered head
379 attachment rate.
380
381

382 **Table 1:** Calculations of Tethered-head attachment rate for different constructs.
383 Dwell times are fit ± 95% CI from Fig. 3 and off-rates are inverse of dwell times with propagated
384 errors. Run Length (RL) in steps are the RL taken from Fig. 2 divided by the step size (8-nm), and
385 errors are ± 95% CI. k_{on}^{TH} were calculated using Eq. 3, with errors propagated from off-rates and
386 RL.

Construct	Dwell Time (s)	Off-rate (s^{-1})	RL in steps (RL/8 nm)	Calc. k_{on}^{TH} (s^{-1})
$1A_{393}$	1.8 ± 0.08	0.56 ± 0.02	375 ± 3	208 ± 8
1A-K1L12	0.3 ± 0.03	3.3 ± 0.3	63 ± 1	208 ± 19
Kin1	1.5 ± 0.1	0.67 ± 0.04	100 ± 3	67 ± 5
K1-1AL12	1.4 ± 0.1	0.71 ± 0.05	113 ± 3	80 ± 6

387

388 **KIF1A run length scales with charge of the K-loop**

389 In principle, swapping in the K-loop of kinesin-1 could be reducing the KIF1A run length either
390 solely due to differences in positive charge, or through some combination of charge and the length
391 of the loop. To test whether the run length data can be accounted for exclusively based on the
392 charge of loop-12, we designed three additional loop-12 mutant constructs having the same length
393 as wild type but having varying net charge in the loop-12 domain. First, we increased the total
394 charge of loop-12 in our $1A_{393}$ construct by replacing three of the native uncharged residues with
395 lysines, resulting in a net charge of +7 in loop-12; we refer to this construct as SuperK (Fig. 4A).
396 Using single-molecule motility assays in BRB80 at 2 mM ATP, we found that the run length of
397 SuperK was ~2-fold longer and the segmented velocity was slightly slower compared to the control
398 $1A_{393}$ (Fig. 4B-C; Table 2). We also used stopped-flow to measure the bimolecular on-rate, k_{on}^{Mt},
399 and found that the SuperK on-rate was 1.5-fold faster than $1A_{393}$, but the values were within fit
400 error of one another (Fig. 4D).
401
402 Next, to test whether reducing the net charge of loop-12 reduces the run length, we replaced a
403 portion of the of the lysine residues in loop-12 with glutamines. Glutamine was chosen because it
404 is uncharged in our buffer (pH 6.9) and the side chain is of similar size to lysine, minimizing
405 potential steric effects. We substituted four or five lysines in $1A_{393}$ by glutamines, creating 4Q and
406 5Q, which had net charges in Loop-12 of 0 and -1, respectively (Fig. 4A). In BRB80 buffer, we

407 observed no processive events for 4Q or 5Q (Fig. 4A; ND, not detected). Thus, although swapping
408 in the kinesin-1 K-loop (K1L12; +1 net charge) led to short but detectable processivity, reducing
409 the net charge of the K-loop further led to undetectable processivity in BRB80 buffer.
410
411 Because lowering the ionic strength enhanced the run length of other KIF1A constructs, we tested
412 the processivity of these K-loop charge mutants in BRB12 buffer and found that they had
413 measurable run lengths under these conditions (see representative kymographs in Fig. S4). This
414 result confirms that the lack of events in BRB80 was not due to protein misfolding or other off-
415 target effects. In BRB12, the run lengths of 4Q and 5Q scaled with the net charge of loop-12, as
416 follows (Fig. 4E). Wild-type $1A_{393}$ (+4 charge) had a run length 14 ± 0.4 μm; K1L12 (+1 charge)
417 had a run length of 6.7 ± 0.1 μm; 4Q (neutral) had a run length of 2.6 ± 0.1 μm; and 5Q (-1 net
418 charge) had a run length of 1.2 ± 0.1 μm) (see also Fig. 6 and Table 3). The velocities in BRB12
419 also differed, but not in a charge-dependent manner (Fig. 4F; Table 3). Interestingly the
420 bimolecular on-rates of the three mutants in BRB12 buffer were similar to one another and they
421 were all ~5-fold slower than $1A_{393}$ (Fig. 4G). Thus, the key feature of KIF1A loop-12 that enhances
422 the motor's processivity is the positive charge rather than the longer length of the loop relative to
423 kinesin-1.

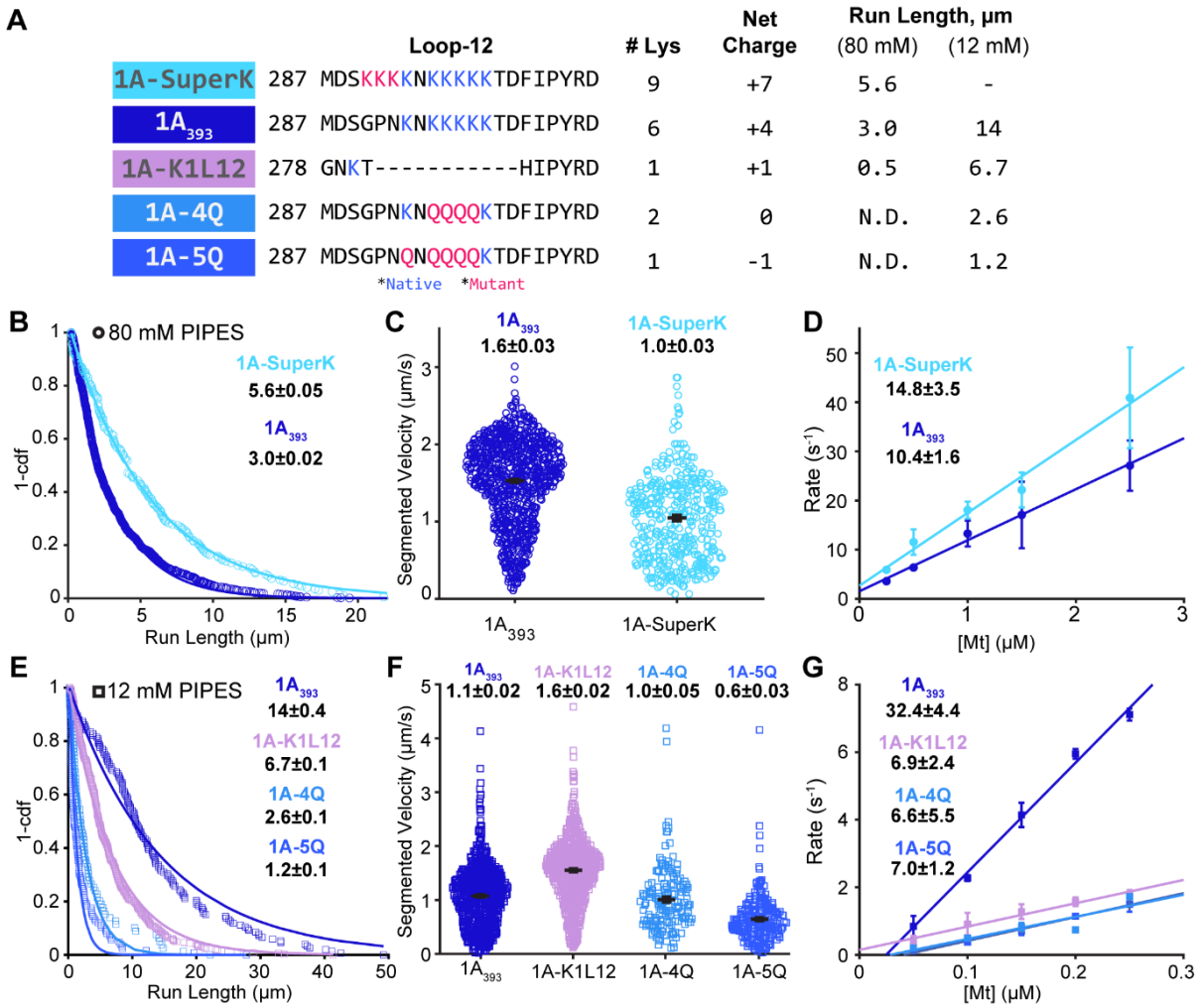

Figure 4: **Charge of the KIF1A K-Loop regulates superprocessivity**

A, Sequence of the Loop-12 domain in the protein constructs used, along with the number of lysine residues and net charge of the domain. Mutations are in red; native lysines are in green. ND indicates not detectable run length. Representative kymographs in Fig. S4. **B,** Run length distribution of $1A_{393}$ (blue circles) and 1A-SuperK (light blue circles) in BRB80 buffer and 2 mM ATP. Values are single exponential fits ± 95% confidence interval. **C,** Velocity distribution of $1A_{393}$ (blue circles) and 1A-SuperK (light blue circles) in BRB80 and 2 mM ATP. Average velocities for segments with $\Delta x > 3$ pixels are mean ± SEM. **D,** Bimolecular on-rates of $1A_{393}$ (blue circles) and 1A-SuperK (light blue circles) in BRB80. Linear fits, reported as fit ± 95% confidence interval, give k_{on}^{Mt}. Points are mean ± SEM. **E,** Run length distribution of $1A_{393}$ (blue squares), 1A-4Q (light blue squares), 5Q (medium blue squares) and 1A-K1L12 (light purple squares) in BRB12 buffer and 2 mM ATP. Values are single exponential fit ± 95% confidence interval. **F,** Velocity

437 distribution of $1A_{393}$ (blue squares), 1A-K1L12 (light purple squares), 1A-4Q (light blue squares),
438 and 1A-5Q (medium blue squares) in BRB12 and 2 mM ATP. Average velocities for segments
439 with $\Delta x > 3$ pixels are reported as mean ± SEM. **G,** Bimolecular on-rates of $1A_{393}$ (blue squares),
440 1A-4Q (light blue squares), 1A-5Q (medium blue squares) and 1A-K1L12 (light purple squares)
441 in BRB12 buffer. Linear fits give k_{on}^{Mt} (fit ± 95% confidence interval). Points are mean ± SEM.

442

443 **Human disease mutations adjacent to the K-loop impair KIF1A motility**

444 To extend our understanding of the role of loop-12 in KIF1A motility, we investigated the motile
445 properties of a set of mutations identified in patients suffering from KIF1A Associated
446 Neurological Disorder (KAND). A recent study investigated the clinical features of 117 KAND
447 patients and identified a number of mutations in the well conserved 'PYRD' sequence at the
448 carboxyl end of loop-12; no patients in the study had mutations in the K-loop proper.[14] We
449 investigated, three pathogenic human mutations: R307P, R307Q, and P305L (Fig. 5A). The four
450 patients harboring the R307Q mutation had moderate to severe KAND with hypertonia/spasticity,
451 and the pair of twins that harbored the R307P mutation displayed brain atrophy and seizures.[13,14]
452 In *C. elegans*, R307Q was able to partially rescue a null mutant;[51] however, to our knowledge the
453 single-molecule properties of R307Q and R307P have not been evaluated. The four patients
454 harboring the P305L mutation ranged from mild to severe KAND; all showed
455 hypertonia/spasticity, but only two of four showed brain atrophy and one of the four exhibited
456 seizures. In contrast to R307Q, P305L was unable to rescue a *C. elegans* null mutant; however,
457 P305L was shown to be motile in single-molecule assays albeit with impaired performance.[52] Thus
458 the P307 mutants, which decrease positive charge near the K-loop, present more severe clinical
459 phenotypes, but the P307Q can partially rescue worms. In contrast, P305L, which has been
460 proposed to alter the conformation of a helix adjacent to the K-loop, has a less severe clinical
461 phenotype and the motor retains some motility, but is unable to rescue mutant worms.[52]

462

463 We first examined R307P, R307Q, and P305L mutants using single-molecule tracking in BRB80
464 and 2 mM ATP, and observed no motility for any of the three disease mutants (Fig. 5B). When the
465 ionic strength was lowered using BRB12 buffer, R307P and R307Q showed a higher frequency of
466 landing events and longer duration of diffusive events, but still no persistent directional movement

467 (Fig. 5B). In contrast, P305L did show processive movement in BRB12, but with a ~5-fold shorter
468 run length and ~2-fold slower velocity than the $1A_{393}$ control in BRB12 (Fig. 5C-D). A previous
469 study found that that the P305L mutation strongly reduced the microtubule landing rate, and
470 suggested that the mutation alters the interaction of the K-Loop with the C-terminal tail of
471 tubulin.[52] To directly measure the microtubule on-rate of P305L, we used the stopped flow k_{on}^{Mt}
472 assay in BRB12 and found that the P305L mutant had a ~3-fold lower on-rate than $1A_{393}$ (Fig. 5E).
473 Interestingly, the P305L on-rate of 9.3 ± 3 $\mu M^{-1}s^{-1}$ (Fig. 5E) was faster than either the loop swap
474 mutant 1A-K1L12 or the two glutamine mutants in BRB12 (Fig. 4G; Table 3). This ~3-fold
475 decrease in the on-rate was in the same direction, but it was much smaller than the ~35-fold
476 decrease in the microtubule landing rate of P305L in previous work.[52]

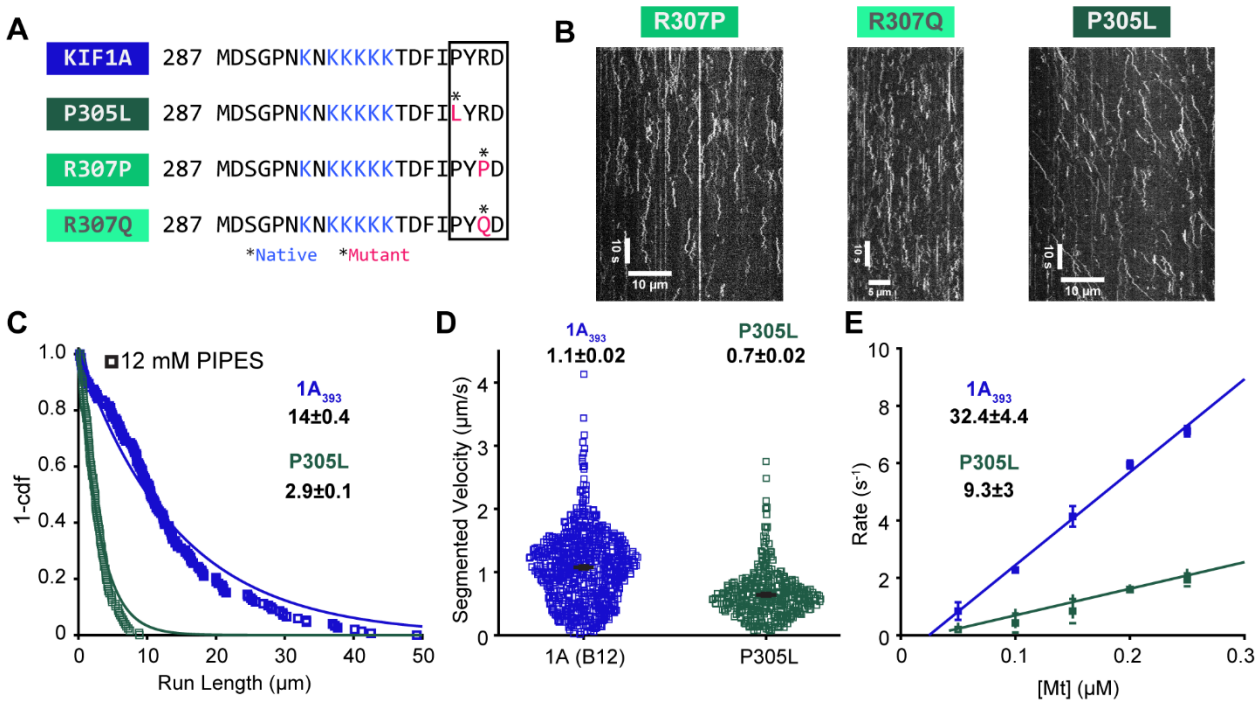

477

478 Figure 5: **Pathogenic mutations in Loop-12 hinder KIF1A motility**

479 **A,** Sequence of the Loop-12 for wild type and mutants, with point mutations indicated in red and
480 conserved distal region indicated by a box. **B,** Example kymographs of R307P, R307Q, and P305L
481 in BRB12 buffer and 2 mM ATP. **C,** Run length distribution of $1A_{393}$ (blue squares) and P305L
482 (green squares) in BRB12 and 2 mM ATP. Values are single exponential fit ± 95% confidence
483 interval. **D,** Velocity distribution of $1A_{393}$ (blue squares) and P305L (green squares) in BRB12 and
484 2 mM ATP. Average velocities for segments with $\Delta x > 3$ pixels are mean ± SEM. **E,** Bimolecular

485 on-rates of $1A_{393}$ (blue squares) and P305L (green squares) in BRB12. Linear fits give k_{on}^{Mt} (fit ±
486 95% confidence interval). Points are mean ± SEM.

487 **Table 2:** Summary of data in BRB80 buffer.

Construct	RL (μm)	Vel (μm/s)	ADP Dwell (s)	k_{on}^{Mt} ($\mu M^{-1} s^{-1}$)
1A(1-393)	3.0 ± 0.02	1.6 ± 0.03 *	1.8 ± 0.08	10.6 ± 0.5
1A-K1L12	0.5 ± 0.004	1.7 ± 0.03	0.3 ± 0.03	9.1 ± 2.5
K1	0.8 ± 0.02	0.7 ± 0.01	1.5 ± 0.1	1.7 ± 0.6
K1-1AL12	0.9 ± 0.02	0.8 ± 0.01	1.4 ± 0.1	9.9 ± 2.9
Super-K	5.6 ± 0.05	1.0 ± 0.03 *	-	14.8 ± 3.5

488 *Segmented Velocity reported.

489

490 **Table 3:** Summary of Data in BRB12 buffer.

Construct	RL (μm)	Vel (μm/s)	k_{on}^{Mt} ($\mu M^{-1} s^{-1}$)
1A(1-393)	14.3 ± 0.4	1.1 ± 0.02 *	32 ± 4.4
1A-K1L12	6.7 ± 0.1	1.6 ± 0.02 *	6.9 ± 2.4
4Q	2.6 ± 0.1	1.0 ± 0.05 *	6.6 ± 5.5
5Q	1.2 ± 0.1	0.6 ± 0.03 *	7.0 ± 1.2
P305L	2.9 ± 0.1	0.7 ± 0.02 *	9.3 ± 3

491 *Segmented Velocity reported.

492

493 **Discussion**

494 The positively charged loop-12 in kinesin-3 motors, known as the K-Loop, has been a topic of
495 interest in the field for many years, but there has yet to be a consensus on the role of the K-loop in
496 the mechanism of KIF1A superprocessivity. In this work, we have established a comprehensive
497 understanding of the mechanism of the K-Loop in the KIF1A chemomechanical cycle. We
498 conclude that the unique superprocessivity of KIF1A dimers originates from the charge-dependent
499 interaction of loop-12 with the microtubule, resulting in a reduction in off-rate from the post-
500 hydrolysis one-head-bound (1HB) state (Fig. 6). This stabilization of the weak-binding state allows
501 time for the tethered head to bind to the next binding site and complete the step, and thus
502 maximizes the number of steps the motor takes before terminating a processive run.

503

504 Despite an appreciation of the importance of the K-loop, there are contradictions in the literature
505 regarding the role of the K-loop in KIF1A superprocessivity. Early work made the striking finding
506 that KIF1A monomer constructs move processively through a combination of intermittent forward
507 steps and 1D diffusion along the microtubule.[25,53] The microtubule affinity of these monomers was
508 shown to depend on the negatively charged C-terminal tail of tubulin, scale with the amount of
509 positive charge in loop-12, and be enhanced in low ionic strength buffers. Subsequently, it was
510 shown that full-length KIF1A is dimeric and the motility of dimer constructs was fast,
511 superprocessive, and lacked the diffusional behavior of the monomers.[30,54] However, using a
512 KIF1A dimer truncated after the neck-coil (1-393 aa), it was found that replacing the KIF1A loop-
513 12 with that of kinesin-1 did not diminish the run length,[31] a result that was puzzling in light of the
514 monomer results. Subsequent work showed that, unlike kinesin-1, the neck-coil domain of KIF1A
515 is insufficient to stably dimerize the motor, and stabilized dimers could be created by adding a
516 leucine zipper sequence downstream of the neck-coil.[19,27,30,32] Upon closer inspection, the apparent
517 lack of influence of loop-12 on KIF1A processivity can be explained by the fact that the construct
518 used in that work (KIF1A(1-393)) lacked a distal coiled-coil region that is needed to stabilize the
519 dimer.[31] In that work, KIF1A(1-393) had a run length of 2.6 μm, the loop-swap mutant had a run
520 length of 3.6 μm, and the stably dimerized KIF1A(1-393)-LZ had a run length of 9.8 μm.[31,32] Thus,
521 the apparent lack of influence of the K-loop in the truncated dimer lacking a stabilizing LZ domain
522 can be explained by run lengths being terminated by the motor reverting to monomers and
523 dissociating from the microtubule rather than termination of a processive run by normal
524 dissociation of the dimer. As a competing process, this premature termination would mask any
525 change in run length due to the loop swap.
526
527 By measuring key transitions in the kinetic race that defines processivity, we find that the principal
528 role of the K-loop is to stabilize the weak-binding, post-hydrolysis state of KIF1A. The finding
529 from the pelleting assay that the K_D for microtubules is similar in ADP and ATP for both wild-
530 type and Loop-12 swapped KIF1A emphasizes the importance of the weak binding state for KIF1A
531 processivity. Their similar residence times are consistent with KIF1A spending the majority of its
532 cycle in a vulnerable one-head-bound ADP state, a key finding from a previous study.[15] The
533 parallel reduction of the microtubule affinity in ADP and ATP upon swapping out the K-loop
534 clearly demonstrates how decreasing the microtubule affinity in the ADP state dictates a reduction

535 in run length. Because the other component of the kinetic race, tethered head attachment, also
536 involves microtubule binding and hence might be expected to be modulated by charge in the K-
537 loop, it was notable that swapping out the K-loop did not alter the tethered head on-rate. Tethered
538 head binding involves both a mechanical component of the tethered head stretching to the next
539 binding site, as well as a biochemical component of ADP release to achieve tight binding, and so
540 the simplest interpretation of this result is that the tethered head binding rate is not substantially
541 mediated by electrostatic interactions between the motor domain and the microtubule.
542 Surprisingly, we found that swapping out the K-loop of KIF1A did not diminish the bimolecular
543 on-rate in solution, meaning that electrostatics mediated by the K-loop do not play a strong role in
544 the initial landing of KIF1A on the microtubule at near physiological ionic strength. This behavior
545 contrasts with kinesin-1, where inserting the K-loop of KIF1A did enhance the bimolecular on-
546 rate in solution, a difference that highlights the different kinetic tuning of the two motor families
547 involved in the initial binding of the motor to the microtubule.

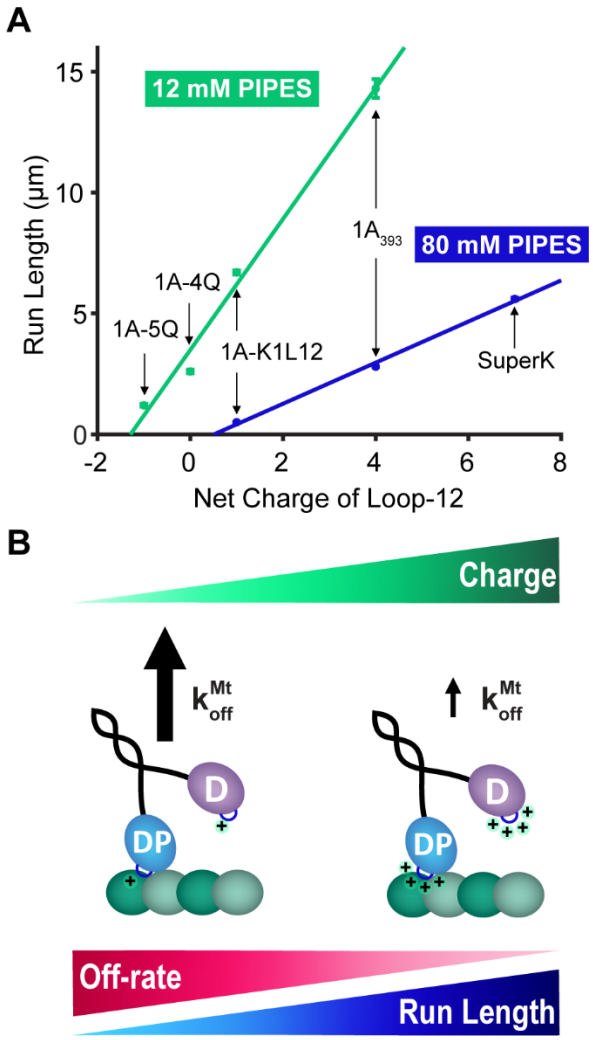

Figure 6: **Run Length of KIF1A is dependent on Charge of Loop-12**

A, Run Length of the various processive constructs used in this study, plotted as a function of the net charge of their Loop-12 domain, in BRB12 and BRB80. Points are from the 1-CDF plots in previous figures (fit ± 95% CI). Linear fits to the points in BRB12 and BRB80 give slopes of 2.7 ± 0.9 and 0.9 ± 0.6, respectively (fit ± 95% CI). **B,** Diagram depicting how increasing positive charge in Loop-12 leads to a slower off-rate in ADP that results in longer run lengths.

By systematically replacing lysines in KIF1A loop-12 with glutamines, we find that the run length of KIF1A scales linearly with the net charge of loop-12 in both BRB80 and BRB12 (Fig. 6). Three published studies using KIF1A or the C. elegans ortholog Unc104 in BRB12 buffer found similarly that reducing the charge of the K-loop by either swapping with the kinesin-1 sequence or replacing lysines with alanines decreased the run length.[27,30,31] Arpag *et. al.* found that swapping the KIF1A

K-loop (net charge +4) with the rat kinesin-1 sequence (net charge +1) caused a 2.2-fold reduction in run length, and Lessard found a 2.6-fold reduction in run length when the net charge of the K-loop was reduced from +4 to +1 by replacing three lysines in the K-loop with alanines.[27] These values are similar to the 2.1-fold reduction in run length we measured between 1A393 (net charge +4) and 1AK1L12 (net charge +1) (Fig. 6A). Using the *C. elegans* KIF1A ortholog Unc104, Tomishige found that swapping the K-loop (net charge +4) with the human kinesin-1 sequence (net charge 0) resulted in a 5.4-fold reduction in run length, which matches our 5.5-fold shorter run length for K1-4Q (net charge 0). The similarity across these studies (shown graphically in Fig. S5) reinforces our finding that KIF1A processivity scales linearly with the charge of the K-loop, and also argues that this reduction does not depend on the specific sequences, but solely due to the electrostatic charge. This linear relationship and x-intercept around a -1 charge also helps to explain why a construct in which all six lysines in the K-loop were replaced with alanines, resulting in a net charge of -2, was not measurably processive.[27,31] Finally, the shallower slope and more positive x-intercept in BRB80 in Fig. 6A is consistent with charge shielding at higher ionic strength reducing the impact of electrostatic interactions on the run length.

We also found that in near-physiological ionic strength buffer, swapping the KIF1A K-loop into kinesin-1 did not confer superprocessivity on this motor (Fig. 2). This result suggests that the KIF1A chemomechanical cycle is tuned such that it relies on the K-loop to achieve superprocessivity, whereas the kinesin-1 chemomechanical cycle is tuned to rely on different mechanisms to achieve processivity. One potential explanation is that because kinesin-1 spends a much smaller fraction of its ATP hydrolysis cycle in a one-head bound vulnerable state than KIF1A,[15,36] altering the microtubule affinity of this state has a negligible effect on the run length. However, the microtubule detachment rate of kinesin-1 in the weak-binding ADP state was not altered by swapping in the KIF1A K-loop (Fig. 3D), arguing against this mechanism and suggesting instead that the positive charge in the K-loop cannot stabilize this vulnerable state in kinesin-1 the way it can in KIF1A. One possibility is that during transient episodes when the motor domain is tethered to the microtubule solely by its K-loop, KIF1A rebinds rapidly through its canonical microtubule binding site to maintain association, whereas kinesin-1 rebinds more slowly and instead dissociates from this tethered state despite the added electrostatic interactions. This difference in weak-binding characteristics suggests that binding of kinesin-1 to the microtubule in

592 the ADP state is dominated by a different region of the microtubule binding domain, such as Loop-
593 8 or Loop-11/α-4.[55]
594
595 There are a number of documented KAND mutations in the well-conserved 'PYRD' sequence at
596 the carboxyl end of loop-12, [14] but how these mutations alter the chemomechanical cycle or the
597 interaction of KIF1A with the microtubule is not clear. Despite a recent report that an R307Q
598 mutant partially rescues vesicle transport in a null-mutant worm,[51] we found that R307Q and
599 R307Q were incapable of productive movement in either BRB80 or BRB12 (Fig. 5). Published
600 molecular dynamics simulations found that R307 in KIF1A (and the equivalent R278 in kinesin-
601 1) interact electrostatically with residues in the tubulin core, and thus likely contribute to the
602 strength of microtubule binding.[55,56] The calculated binding free energies between R307 and
603 residues in tubulin were similar between the strong-binding ATP and Apo states and the weak-
604 binding ADP state in that work,[55] suggesting that R307 is not involved in nucleotide-dependent
605 changes in microtubule binding affinity that occur through the KIF1A mechanochemical cycle.
606 However, the lack of motility of the R307 mutants suggests this residue plays a key role in
607 mechanochemical coupling in the motor domain and/or the strong binding interaction needed for
608 stepping. On the other hand, the diffusive binding of both R307P and R307Q suggest that these
609 mutations do not prevent the K-loop from interacting with the C-terminal tail of tubulin. A nearby
610 mutation, P305L, was previously proposed to alter the interaction of the K-loop with the
611 microtubule based on a ~35-fold reduction in the single-molecule landing rate.[52] That work was
612 carried out in a ~160 mM ionic strength HEPES buffer at pH 7.4, though a different study using
613 ~80 mM ionic strength HEPES buffer at pH 7.2 found only a two-fold decrease in the landing rate.
614 [14] Using a biochemical assay in BRB12 (26 mM ionic strength, pH 6.9) that is robust to variations
615 in motor activity between constructs, we found a 3.5-fold decrease in the bimolecular on-rate for
616 P305L. This on-rate suppression was smaller than the effect of mutations that neutralized the
617 charge of the K-loop (see Table 3), which suggests that at low ionic strength the P305L mutation
618 does not inhibit the interaction of the K-loop with the C-terminal tail of tubulin. Notably, we failed
619 to observe any motility of P305L in BRB80 (173 mM ionic strength, pH 6.9), which is consistent
620 with the inability of P305L to rescue vesicle motility in a null worm.[52] Hence, the effect of
621 different KAND mutations on microtubule binding and chemomechanical coupling are highly
622 dependent on experimental conditions, and further work is needed to connect the structural

623 changes with alterations in motility, as well as how changes in the motile properties translate to
624 defects in axonal transport.
625
626 The present study highlights different chemomechanical tuning strategies that kinesin-1 and
627 kinesin-3 employ to carry out their intracellular transport functions. KIF1A is notable in being fast
628 and superprocessive, and it does this by spending most of its hydrolysis cycle in a vulnerable one-
629 head-bound state that is stabilized by electrostatic interactions between the K-loop and the
630 microtubule. Importantly, this strategy causes the motor to detach readily under load, which is
631 seemingly not an advantageous property for a transport motor.[19–22] However, KIF1A binds to the
632 microtubule from solution at a much faster rate than kinesin-1, which may partly compensate for
633 this detachment.[15] In contrast, kinesin-1 is able to walk processively against substantial loads,[20,22]
634 but it walks more slowly, it binds to the microtubule out of solution more slowly, and in the absence
635 of load has a considerably shorter run length.[15,31] As the mechanistic features of these motors
636 become clarified, the next step is to understand how these functional properties scale up to
637 multimotor cargo transport on diverse microtubules and bidirectional tug-of-war transport with
638 dynein. Similarly, to understand how specific mutations lead to KAND disease states, it will be
639 necessary to define the effect of other mutations on KIF1A chemomechanics and to extrapolate
640 how those changes affect neuronal function.

641 **Methods**

642 *Protein Preparation*

643

644 *Rattus norvegicus* KIF1A motor constructs were based on previous work.[15] The $1A_{393}$ construct,
645 used as the 'wild type' throughout this study, included the KIF1A motor head, neck linker, and
646 neck-coil domains (residues 1-393) followed by the *D. melanogaster* kinesin-1 neck-coil and
647 coiled-coil 1 domains (residues 345 to 560), and C-terminal GFP tag for single-molecule assays,
648 or *D. melanogaster* kinesin-1 neck-coil (residues 345 to 406) for biochemical assays. The $1A_{368}$
649 construct consisted of the KIF1A motor head and the neck linker domains (residues 1-368)
650 followed by the *D. melanogaster* kinesin-1 coil domains for stable dimerization (same residues
651 and tags as used above for $1A_{393}$). The 1A-LZ construct was composed of *R. norvegicus* KIF1A
652 residues 1-393 followed by a leucine zipper domain (see Fig. S2 for sequence) for stable
653 dimerization and a C-terminal GFP tag.[32] Subsequent constructs used throughout this study
654 introduced mutations (as described in the Results) using the $1A_{393}$ construct as the template. All
655 proteins contained a C-terminal His_6 tag. Plasmids were designed in SnapGene and mutants were
656 generated via Gibson assembly (Gibson Assembly® Cloning Kit from New England Biolabs)[57,58]
657 or via QuickChange (Q5® Site-Directed Mutagenesis Kit from New England Biolabs).[59]
658 Recombinant expression of motors in *E. coli* and purification via Ni-NTA chromatography were
659 performed as described previously.[15]

660

661 *Single Molecule Fluorescence Tracking*

662 Single-molecule TIRF microscopy assays were performed as previously described.[15,40,42] Flow
663 cells were injected sequentially with casein for surface blocking, rigor motors for binding
664 microtubules to the surface,[36] and taxol-stabilized microtubules in BRB80 (80 mM PIPES, 1 mM
665 EGTA, 1 mM $MgCl_2$, pH 6.9). The imaging buffer mixture was BRB80 with 20 mM D-glucose,
666 0.02 mg/ml glucose oxidase, 0.008 mg/ml catalase, and 10 mM DTT (dithiothreitol). Motors were
667 diluted in imaging buffer with 0.5 mg/ml casein and 2 mM ADP/ATP (and equal molar $MgCl_2$).
668 Videos were recorded at 10 frames per second in most cases, except 20 or 50 fps in ADP and
669 BRB80 and 5 fps in ADP or ATP and BRB12. Kymograph analysis was carried out manually with
670 ImageJ. To eliminate bias, all traces below 3 pixels (along the distance axis for ATP assays and
671 the time axis for ADP assays) were excluded from the data set. Fits to the data distributions were

672 done using MATLAB R2020b (MathWorks). The cutoff for the fits in the 1-CDF plots was
673 determined as 3x the pixel value (i.e. 0.17 μm for run length in ATP assays or 0.3 s for ADP dwell
674 time assays done at 10 fps). Statistical analysis was carried out using GraphPad Prism7 t-test
675 function (Kolmogorov-Smirnov test) to determine significance relative to the control.
676
677 *Stopped Flow Assays*
678 Stopped Flow assays, including k_{on}^{Mt} and ATP-triggered Half-Site Release were performed as
679 previously described.[15] Concentrations mentioned below refer to the 'syringe concentrations' and
680 the final concentrations in the chamber were half. The k_{on}^{Mt} assays in BRB80 were performed by
681 flushing 300 nM of active motor dimers in 0.5 μM mant-ADP against 2 mM Mg-ADP and varying
682 concentrations of taxol-stabilized microtubules (0.5 - 5 μM). In BRB12, 300 nM of active motor
683 dimers in 5 μM mant-ADP were flushed against 2 mM Mg-ATP and varying concentrations of
684 taxol-stabilized microtubules (0.1 – 0.5 μM). The ATP-triggered Half-Site Release assays were
685 performed by incubating 0.5 μM active motor dimers with 6 μM of taxol-stabilized microtubules
686 and 1 μM of excess mant-ADP to form a one-head-bound complex in solution. This complex was
687 then flushed against varied concentrations of Mg-ATP.
688
689 *Microtubule Pelleting Assays*
690 In microtubule pelleting assays, GFP-labeled motors were incubated with varying concentrations
691 of taxol-stabilized microtubules with 2 mM ADP or ATP. After a 5 minute incubation at room
692 temperature, the solutions were spun down using an Airfuge at 30 psi for 10 minutes. A Molecular
693 Devices FlexStation 3 Multimode Microplate Reader was used to measure the GFP concentration
694 of the pellet and supernatant. Reported values (% pellet) were calculated as the fluorescence of the
695 pellet divided by the sum of the pellet and supernatant. All values were normalized to a control
696 value of motors in 2 mM AMPPNP and 20 μM taxol-stabilized microtubules.

697 **References**

698 (1) Hirokawa, N., Noda, Y. Intracellular Transport and Kinesin Superfamily Proteins,
699 KIFs: Structure, Function, and Dynamics. *Physiol Rev* **2008**, *88* (3), 1089–1118.
700 (2) Miki, H., Setou, M., Kaneshiro, K., Hirokawa, N. All Kinesin Superfamily Protein,
701 KIF, Genes in Mouse and Human. *Proceedings of the National Academy of Sciences*
702 **2001**, *98* (13), 7004–7011.
703 (3) Hirokawa, N., Noda, Y., Tanaka, Y., Niwa, S. Kinesin Superfamily Motor Proteins
704 and Intracellular Transport. *Nat Rev Mol Cell Biol* **2009**, *10*, 682–696.
705 (4) Niwa, S., Lipton, D. M., Morikawa, M., Zhao, C., Hirokawa, N., Lu, H., Shen, K.
706 Autoinhibition of a Neuronal Kinesin UNC-104/KIF1A Regulates the Size and
707 Density of Synapses. *Cell Rep* **2016**, *16* (8), 2129–2141.
708 (5) Yonekawa, Y., Harada, A., Okada, Y., Funakoshi, T., Kanai, Y., Takei, Y., Terada,
709 S., Noda, T., Hirokawa, N. Defect in Synaptic Vesicle Precursor Transport and
710 Neuronal Cell Death in KIF1A Motor Protein–Deficient Mice. *Journal of Cell*
711 *Biology* **1998**, *141* (2), 431–441.
712 (6) Vecchia, S. della, Tessa, A., Dosi, C., Baldacci, J., Pasquariello, R., Antenora, A.,
713 Astrea, G., Bassi, M. T., Battini, R., Casali, C., Cioffi, E., Conti, G., de Michele, G.,
714 Ferrari, A. R., Filla, A., Fiorillo, C., Fusco, C., Gallone, S., Germiniasi, C., Guerrini,
715 R., Haggiag, S., Lopergolo, D., Martinuzzi, A., Melani, F., Mignarri, A., Panzeri, E.,
716 Pini, A., Pinto, A. M., Pochiero, F., Primiano, G., Procopio, E., Renieri, A.,
717 Romaniello, R., Sancricca, C., Servidei, S., Spagnoli, C., Ticci, C., Rubegni, A.,
718 Santorelli, F. M. Monoallelic KIF1A-Related Disorders: A Multicenter Cross
719 Sectional Study and Systematic Literature Review. *J Neurol* **2022**, *269* (1), 437–450.
720 (7) Anazawa, Y., Kita, T., Iguchi, R., Hayashi, K., Niwa, S. De Novo Mutations in
721 KIF1A-Associated Neuronal Disorder (KAND) Dominant-Negatively Inhibit Motor
722 Activity and Axonal Transport of Synaptic Vesicle Precursors. *Proceedings of the*
723 *National Academy of Sciences* **2022**, *119* (32).
724 (8) Esmaeeli Nieh, S., Madou, M. R. Z. Z., Sirajuddin, M., Fregeau, B., McKnight, D.,
725 Lexa, K., Strober, J., Spaeth, C., Hallinan, B. E., Smaoui, N., Pappas, J. G., Burrow,
726 T. A., McDonald, M. T., Latibashvili, M., Leshinsky-Silver, E., Lev, D., Blumkin,
727 L., Vale, R. D., Barkovich, A. J., Sherr, E. H. De Novo Mutations in KIF1A Cause

728 Progressive Encephalopathy and Brain Atrophy. *Ann Clin Transl Neurol* **2015**, *2* (6),
729 623–635.
730 (9) Pennings, M., Schouten, M. I., van Gaalen, J., Meijer, R. P. P. P., de Bot, S. T., Kriek,
731 M., Saris, C. G. J. J., van den Berg, L. H., van Es, M. A., Zuidgeest, D. M. H. H.,
732 Elting, M. W., van de Kamp, J. M., van Spaendonck-Zwarts, K. Y., Die-Smulders,
733 C. de, Brilstra, E. H., Verschuuren, C. C., de Vries, B. B. A. A., Bruijn, J., Sofou, K.,
734 Duijkers, F. A., Jaeger, B., Schieving, J. H., van de Warrenburg, B. P., Kamsteeg,
735 E.-J. KIF1A Variants Are a Frequent Cause of Autosomal Dominant Hereditary
736 Spastic Paraplegia. *European Journal of Human Genetics* **2020**, *28* (1), 40–49.
737 (10) Ohba, C., Haginoya, K., Osaka, H., Kubota, K., Ishiyama, A., Hiraide, T., Komaki,
738 H., Sasaki, M., Miyatake, S., Nakashima, M., Tsurusaki, Y., Miyake, N., Tanaka, F.,
739 Saitsu, H., Matsumoto, N. De Novo KIF1A Mutations Cause Intellectual Deficit,
740 Cerebellar Atrophy, Lower Limb Spasticity and Visual Disturbance. *J Hum Genet*
741 **2015**, *60* (12), 739–742.
742 (11) Krenn, M., Zulehner, G., Hotzy, C., Rath, J., Stogmann, E., Wagner, M., Haack, T.
743 B., Strom, T. M., Zimprich, A., Zimprich, F. Hereditary Spastic Paraplegia Caused
744 by Compound Heterozygous Mutations Outside the Motor Domain of the KIF1A
745 Gene. *Eur J Neurol* **2017**, *24* (5), 741–747.
746 (12) Hotchkiss, L., Donkervoort, S., Leach, M. E., Mohassel, P., Bharucha-Goebel, D. X.,
747 Bradley, N., Nguyen, D., Hu, Y., Gurgel-Giannetti, J., Bönnemann, C. G. Novel de
748 Novo Mutations in KIF1A as a Cause of Hereditary Spastic Paraplegia with
749 Progressive Central Nervous System Involvement. *J Child Neurol* **2016**, *31* (9),
750 1114–1119.
751 (13) Nemani, T., Steel, D., Kaliakatsos, M., DeVile, C., Ververi, A., Scott, R., Getov, S.,
752 Sudhakar, S., Male, A., Mankad, K., Muntoni, F., Reilly, M. M., Kurian, M. A., Carr,
753 L., Munot, P. KIF1A -related Disorders in Children: A Wide Spectrum of Central
754 and Peripheral Nervous System Involvement. *Journal of the Peripheral Nervous*
755 *System* **2020**, *25* (2), 117–124.
756 (14) Boyle, L., Rao, L., Kaur, S., Fan, X., Mebane, C., Hamm, L., Thornton, A.,
757 Ahrendsen, J. T., Anderson, M. P., Christodoulou, J., Gennerich, A., Shen, Y.,
758 Chung, W. K. Genotype and Defects in Microtubule-Based Motility Correlate with

759 Clinical Severity in KIF1A-Associated Neurological Disorder. *Human Genetics and*
760 *Genomics Advances* **2021**, *2* (2), 100026.
761 (15) Zaniewski, T. M., Gicking, A. M., Fricks, J., Hancock, W. O. A Kinetic Dissection
762 of the Fast and Superprocessive Kinesin-3 KIF1A Reveals a Predominant One-Head-
763 Bound State during Its Chemomechanical Cycle. *Journal of Biological Chemistry*
764 **2020**, *295* (52), 17889–17903.
765 (16) Taylor, E. W., Borisy, G. G. Kinesin Processivity. *Journal of Cell Biology* **2000**, *151*
766 (5), 1998–2000.
767 (17) Mickolajczyk, K. J., Hancock, W. O. Kinesin Processivity Is Determined by a Kinetic
768 Race from a Vulnerable One-Head-Bound State. *Biophys J* **2017**, *112* (12), 2615–
769 2623.
770 (18) Hancock, W. O., Howard, J. Kinesin's Processivity Results from Mechanical and
771 Chemical Coordination between the ATP Hydrolysis Cycles of the Two Motor
772 Domains. *Proc Natl Acad Sci U S A* **1999**, *96* (23), 13147–13152.
773 (19) Arpağ, G., Norris, S. R., Mousavi, S. I., Soppina, V., Verhey, K. J., Hancock, W. O.,
774 Tüzel, E. Motor Dynamics Underlying Cargo Transport by Pairs of Kinesin-1 and
775 Kinesin-3 Motors. *Biophys J* **2019**, *116* (6), 1115–1126.
776 (20) Pyrpassopoulosa, S., Gicking, A. M., Zaniewski, T. M., Hancock, W. O., Ostapa, E.
777 M. KIF1A Is Kinetically Tuned to Be a Super-Engaging Motor under Hindering
778 Loads. *bioRxiv* **2022**, No. 2022.05.16.492183, 1–45.
779 (21) Arpağ, G., Shastry, S., Hancock, W. O., Tüzel, E. Transport by Populations of Fast
780 and Slow Kinesins Uncovers Novel Family-Dependent Motor Characteristics
781 Important for In Vivo Function. *Biophys J* **2014**, *107* (8), 1896–1904.
782 (22) Budaitis, B. G., Jariwala, S., Rao, L., Yue, Y., Sept, D., Verhey, K. J., Gennerich, A.
783 Pathogenic Mutations in the Kinesin-3 Motor KIF1A Diminish Force Generation and
784 Movement through Allosteric Mechanisms. *Journal of Cell Biology* **2021**, *220* (4).
785 (23) Okada, Y., Hirokawa, N. A Processive Single-Headed Motor: Kinesin Superfamily
786 Protein KIF1A. *Science* **1999**, *283* (5405), 1152–1157.
787 (24) Okada, Y., Higuchi, H., Hirokawa, N. Processivity of the Single-Headed Kinesin
788 KIF1A through Binding to Tubulin. *Nature* **2003**, *424* (6948), 574–577.

789 (25) Okada, Y., Hirokawa, N. Mechanism of the Single-Headed Processivity: Diffusional
790 Anchoring between the K-Loop of Kinesin and the C Terminus of Tubulin.
791 *Proceedings of the National Academy of Sciences* **2000**, *97* (2), 640–645.
792 (26) Nitta, R., Kikkawa, M., Okada, Y., Hirokawa, N. KIF1A Alternately Uses Two
793 Loops to Bind Microtubules. *Science* **2004**, *305* (5684), 678–683.
794 (27) Lessard, D. v., Zinder, O. J., Hotta, T., Verhey, K. J., Ohi, R., Berger, C. L.
795 Polyglutamylation of Tubulin's C-Terminal Tail Controls Pausing and Motility of
796 Kinesin-3 Family Member KIF1A. *Journal of Biological Chemistry* **2019**, *294* (16),
797 6353–6363.
798 (28) Janke, C., Magiera, M. M. The Tubulin Code and Its Role in Controlling Microtubule
799 Properties and Functions. *Nat Rev Mol Cell Biol* **2020**, *21* (6), 307–326.
800 (29) Roll-Mecak, A. The Tubulin Code in Microtubule Dynamics and Information
801 Encoding. *Dev Cell* **2020**, *54* (1), 7–20.
802 (30) Tomishige, M., Klopfenstein, D. R., Vale, R. D. Conversion of Unc104/KIF1A
803 Kinesin into a Processive Motor After Dimerization. *Science* **2002**, *297* (5590),
804 2263–2267.
805 (31) Soppina, V., Verhey, K. J. The Family-Specific K-Loop Influences the Microtubule
806 on-Rate but Not the Superprocessivity of Kinesin-3 Motors. *Mol Biol Cell* **2014**, *25*
807 (14), 2161–2170.
808 (32) Soppina, V., Norris, S. R., Dizaji, A. S., Kortus, M., Veatch, S., Peckham, M.,
809 Verhey, K. J. Dimerization of Mammalian Kinesin-3 Motors Results in
810 Superprocessive Motion. *Proceedings of the National Academy of Sciences* **2014**,
811 *111* (15), 5562–5567.
812 (33) Ren, J., Wang, S., Chen, H., Wang, W., Huo, L., Feng, W. Coiled-Coil 1-Mediated
813 Fastening of the Neck and Motor Domains for Kinesin-3 Autoinhibition.
814 *Proceedings of the National Academy of Sciences* **2018**, *115* (51), E11933–E11942.
815 (34) Ren, J., Zhang, Y., Wang, S., Huo, L., Lou, J., Feng, W. Structural Delineation of the
816 Neck Linker of Kinesin-3 for Processive Movement. *J Mol Biol* **2018**, *430* (14),
817 2030–2041.

818 (35) Feng, Q., Mickolajczyk, K. J., Chen, G.-Y., Hancock, W. O. Motor Reattachment
819 Kinetics Play a Dominant Role in Multimotor-Driven Cargo Transport. *Biophys J*
820 **2018**, *114* (2), 400–409.
821 (36) Mickolajczyk, K. J., Deffenbaugh, N. C., Ortega Arroyo, J., Andrecka, J., Kukura,
822 P., Hancock, W. O. Kinetics of Nucleotide-Dependent Structural Transitions in the
823 Kinesin-1 Hydrolysis Cycle. *Proceedings of the National Academy of Sciences* **2015**,
824 *112* (52), E7186–E7193.
825 (37) Huang, T.-G., Suhan, J., Hackney, D. D. Drosophila Kinesin Motor Domain
826 Extending to Amino Acid Position 392 Is Dimeric When Expressed in Escherichia
827 Coli. *J Biol Chem* **1994**, *269* (23), 16502–16507.
828 (38) Thorn, K. S., Ubersax, J. A., Vale, R. D. Engineering the Processive Run Length of
829 the Kinesin Motor. *Journal of Cell Biology* **2000**, *151* (5), 1093–1100.
830 (39) Hughes, J., Hancock, W. O., Fricks, J. Kinesins with Extended Neck Linkers: A
831 Chemomechanical Model for Variable-Length Stepping. *Bull Math Biol* **2012**, *74* (5),
832 1066–1097.
833 (40) Shastry, S., Hancock, W. O. Neck Linker Length Determines the Degree of
834 Processivity in Kinesin-1 and Kinesin-2 Motors. *Current Biology* **2010**, *20* (10), 939–
835 943.
836 (41) Shastry, S., Hancock, W. O. Interhead Tension Determines Processivity across
837 Diverse N-Terminal Kinesins. *Proceedings of the National Academy of Sciences*
838 **2011**, *108* (39), 16253–16258.
839 (42) Chen, G.-Y., Arginteanu, D. F. J., Hancock, W. O. Processivity of the Kinesin-2
840 KIF3A Results from Rear Head Gating and Not Front Head Gating. *Journal of*
841 *Biological Chemistry* **2015**, *290* (16), 10274–10294.
842 (43) Hariharan, V., Hancock, W. O. Insights into the Mechanical Properties of the Kinesin
843 Neck Linker Domain from Sequence Analysis and Molecular Dynamics Simulations.
844 *Cell Mol Bioeng* **2009**, *2* (2), 177–189.
845 (44) Kozielski, F., Sack, S., Marx, A., Thorma, M. The Crystal Structure of Dimeric
846 Kinesin and Implications for Microtubule-Dependent Motility. **1997**, *91*, 985–994.

847 (45) Mouat, M. F., Manchester, K. L. The Intracellular Ionic Strength of Red Cells and
848 the Influence of Complex Formation. *Comparative Haematology International* **1998**,
849 *8* (1), 58–60.
850 (46) Dill, K. A., Bromberg, S., Stigter, D. *Molecular Driving Forces: Statistical*
851 *Thermodynamics in Biology, Chemistry, Physics, and Nanoscience*; Garland Science,
852 2010.
853 (47) Cheng, J. Q., Jiang, W., Hackney, D. D. Interaction of Mant-Adenosine Nucleotides
854 and Magnesium with Kinesin. *Biochemistry* **1998**, *37* (15), 5288–5295.
855 (48) Hackney, D. D., Malik, A. S., Wright, K. W. Nucleotide-Free Kinesin Hydrolyzes
856 ATP with Burst Kinetics. *J Biol Chem* **1989**, *264* (27), 15943–15948.
857 (49) Hackney, D. D. Evidence for Alternating Head Catalysis by Kinesin during
858 Microtubule-Stimulated ATP Hydrolysis. *Proc Natl Acad Sci U S A* **1994**, *91* (15),
859 6865–6869.
860 (50) Ma, Y.-Z., Taylor, E. W. Interacting Head Mechanism of Microtubule-Kinesin
861 ATPase. *Journal of Biological Chemistry* **1997**, *272* (2), 724–730.
862 (51) Chiba, K., Takahashi, H., Chen, M., Obinata, H., Arai, S., Hashimoto, K., Oda, T.,
863 McKenney, R. J., Niwa, S. Disease-Associated Mutations Hyperactivate KIF1A
864 Motility and Anterograde Axonal Transport of Synaptic Vesicle Precursors.
865 *Proceedings of the National Academy of Sciences* **2019**, *116* (37), 18429–18434.
866 (52) Lam, A. J., Rao, L., Anazawa, Y., Okada, K., Chiba, K., Dacy, M., Niwa, S.,
867 Gennerich, A., Nowakowski, D. W., McKenney, R. J. A Highly Conserved 310 Helix
868 within the Kinesin Motor Domain Is Critical for Kinesin Function and Human
869 Health. *Sci Adv* **2021**, *7* (18), 1–15.
870 (53) Hirokawa, N. Kinesin and Dynein Superfamily Proteins and the Mechanism of
871 Organelle Transport. *Science* **1998**, *279* (5350), 519–526.
872 (54) Rashid, D. J., Bononi, J., Tripet, B. P., Hodges, R. S., Pierce, D. W. Monomeric and
873 Dimeric States Exhibited by the Kinesin-Related Motor Protein KIF1A. *Journal of*
874 *Peptide Research* **2005**, *65* (6), 538–549.
875 (55) Scarabelli, G., Soppina, V., Yao, X. Q., Atherton, J., Moores, C. A., Verhey, K. J.,
876 Grant, B. J. Mapping the Processivity Determinants of the Kinesin-3 Motor Domain.
877 *Biophys J* **2015**, *109* (8), 1537–1540.

878 (56) Grant, B. J., Gheorghe, D. M., Zheng, W., Alonso, M., Huber, G., Dlugosz, M.,
879 McCammon, J. A., Cross, R. A. Electrostatically Biased Binding of Kinesin to
880 Microtubules. *PLoS Biol* **2011**, *9* (11), 1001207.
881 (57) Gibson, D. G., Glass, J. I., Lartigue, C., Noskov, V. N., Chuang, R. Y., Algire, M.
882 A., Benders, G. A., Montague, M. G., Ma, L., Moodie, M. M., Merryman, C., Vashee,
883 S., Krishnakumar, R., Assad-Garcia, N., Andrews-Pfannkoch, C., Denisova, E. A.,
884 Young, L., Qi, Z. N., Segall-Shapiro, T. H., Calvey, C. H., Parmar, P. P., Hutchison,
885 C. A., Smith, H. O., Venter, J. C. Creation of a Bacterial Cell Controlled by a
886 Chemically Synthesized Genome. *Science* **2010**, *329* (5987), 52–56.
887 (58) Gibson, D. G., Young, L., Chuang, R. Y., Venter, J. C., Hutchison, C. A., Smith, H.
888 O. Enzymatic Assembly of DNA Molecules up to Several Hundred Kilobases. *Nat*
889 *Methods* **2009**, *6* (5), 343–345.
890 (59) Papworth, C., Bauer, J. C., Braman, J., Wright, D. A. Site-Directed Mutagenesis in
891 One Day with >80% Efficiency. *Strategies* **1996**, *9* (3), 3–4.
892

The net charge of the K-loop regulates KIF1A superprocessivity by enhancing microtubule affinity in the one-head-bound state

Taylor M. Zaniewski and William O. Hancock

Departments of Chemistry and Biomedical Engineering, Pennsylvania State University, University Park, Pennsylvania, USA

Supplemental Information

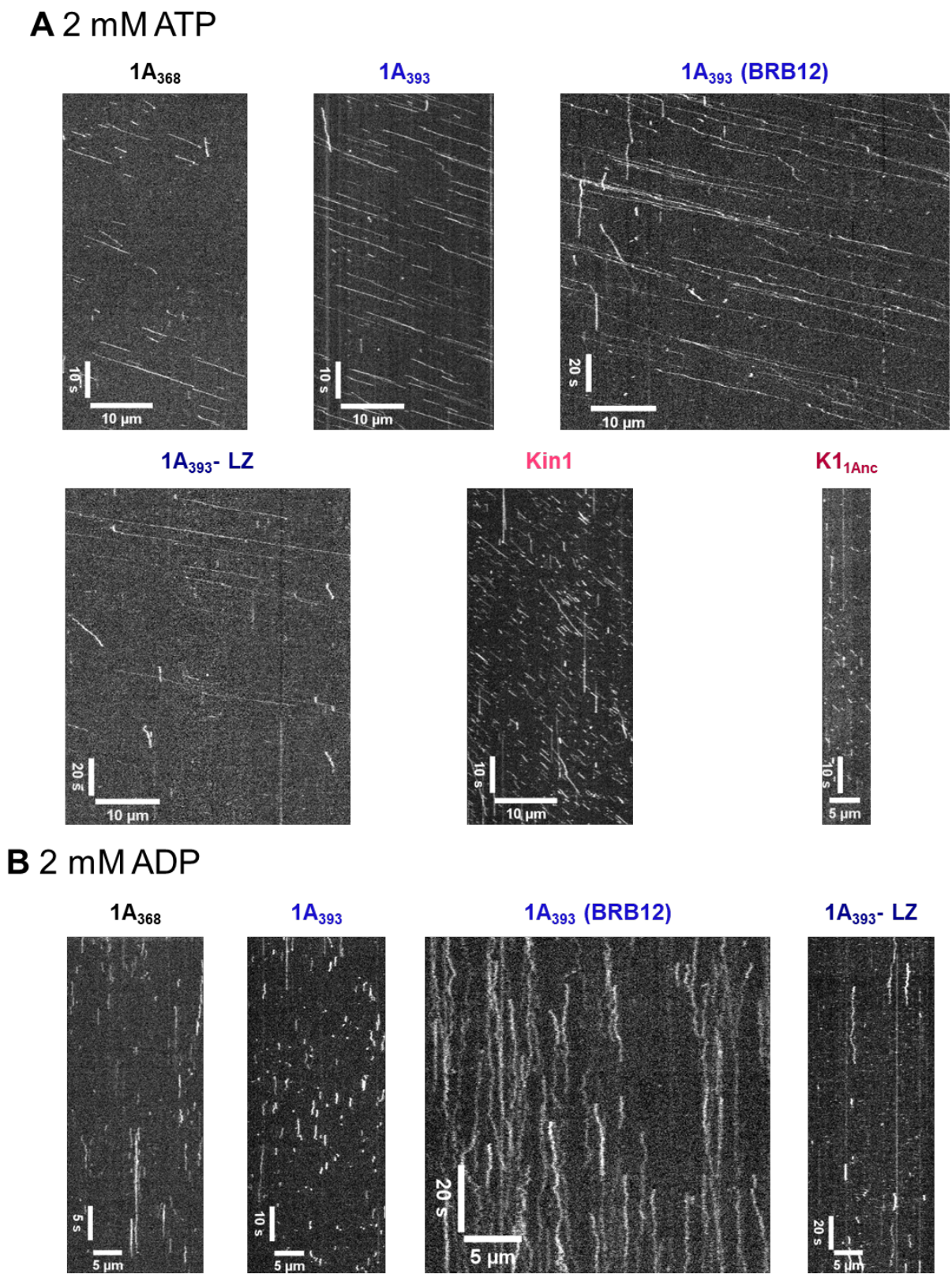

Figure S1: **Example kymographs for different KIF1A and Kin1 constructs in ATP and ADP**

A, Kymograph of each construct in 2 mM ATP and BRB80 (unless otherwise noted). **B,** Kymograph of each construct in 2 mM ADP and BRB80 (unless otherwise noted). Individual kymographs were analyzed from videos at various frame rates; scale bars reflect this distinction.

	Domain	Sequence	Total Charges	Net Charge at pH 6.9	pI
Dimerization Domains	**LZ**	VKQLEDKVEELASKNYHLENEVARLKKLVG	(+7, -6)	+ 0.2	7.2
	LZ + Linker	GAGVKQLEDKVEELASKNYHLENEVARLKKLV GVPRAMLVPRGPVHRLGDPPVAT	(+11, -7)	+ 2.5	9.3
	K560 (345-560)	AEEWKRRYEKEKEKNARLKGKVEKLEIELARW RAGETVKAEEQINMEDLMEASTPNLEVEAAQT AAAEAALAAQRTALANMSASVAVNEQARLATE CERLYQQLDDKDEEINQQSQYAEQLKEQVMEQ EELIANARREYETLQSEMARIQQENESAKEEV KEVLQALEELTVNYDQKSQEIDNKNKDIDALN EELQQKQSVFNAASTELQQLKDMS	(+28, -49)	- 21	4.5
	KIF1A CC1 (394-523)	MTNALVGMSPSSSLSALSSRAASVSSLHERIL FAPGSEEAIERLKETEKIIAELNETWEEKLRR TEAIRMEREALLAEMGVAMREDGGTLGVFSPK KTPHLVNLNEDPLMSECLLYYIKDGVTRVGRE DA	(+16, -22)	- 5.5	5
Neck Coil Domains	**Kin1 Neck Coil** (345-405)	AEEWKRRYEKEKEKNARLKGKVEKLEIELARW RAGETVKAEEQINMEDLMEASTPNLEVEAS	(+13, -16)	- 3.0	5.0
	KIF1A Neck Coil (369-393)	IRELKDEVTRLRDLLYAQGLGDITD	(+4, -6)	- 2.1	4.7
	KIF1A NC+CC1 (369-523)	IRELKDEVTRLRDLLYAQGLGDITDMTNALVG MSPSSSLSALSSRAASVSSLHERILFAPGSEE AIERLKETEKIIAELNETWEEKLRRTEAIRME REALLAEMGVAMREDGGTLGVFSPKKTPHLVN LNEDPLMSECLLYYIKDGVTRVGREDA	(+20, -28)	- 7.4	5.0

Figure S2: **Charge of the neck coil domains impacts motor properties of KIF1A**

A, Table of the different dimerization and neck coil domains used in this study with the sequence, total number of charged residues, net charge of the domain at pH 6.9 and the pI. Net charge and pI were calculated using (http://protcalc.sourceforge.net/)

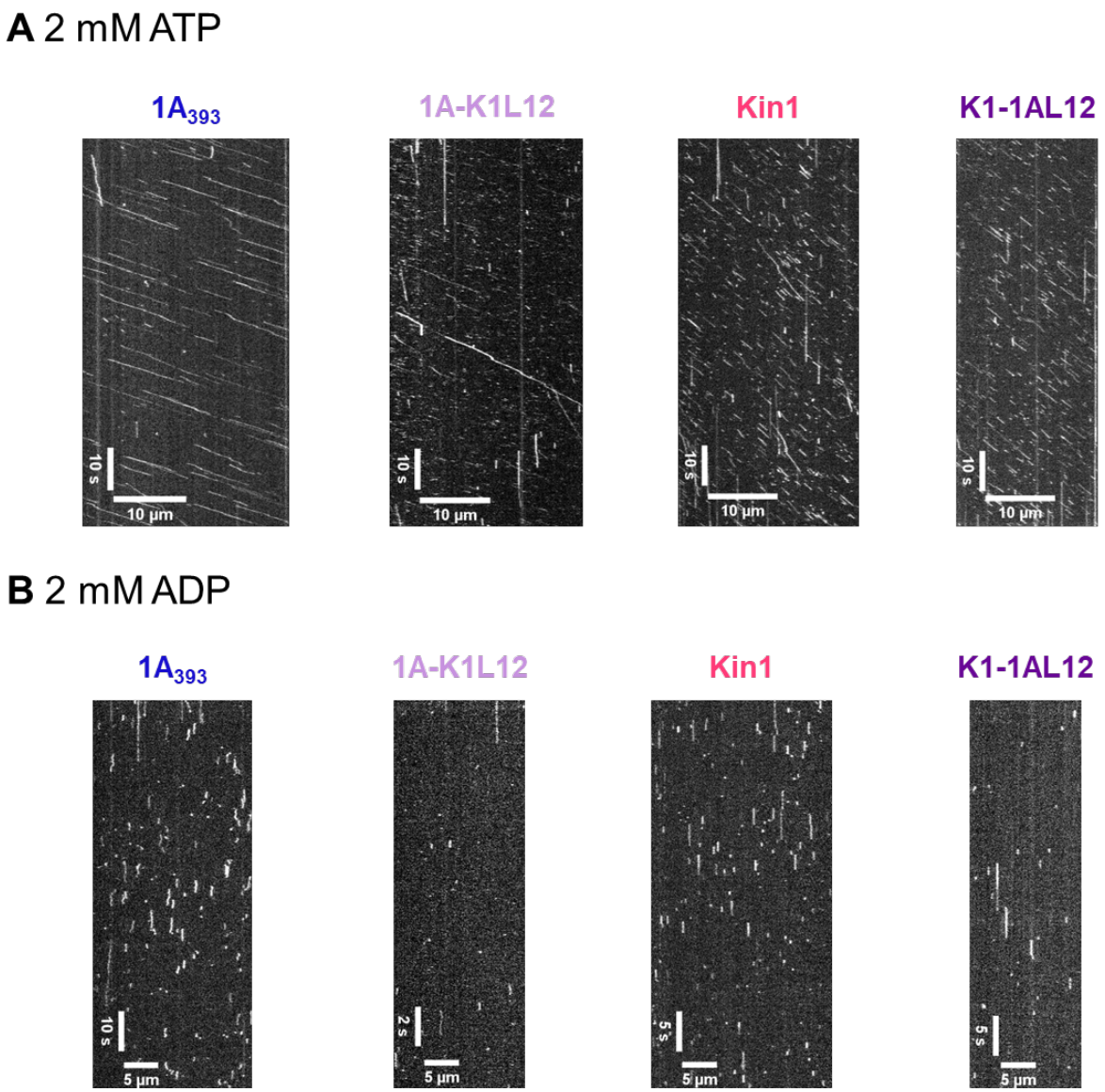

Figure S3: **Example kymographs of constructs in ATP and ADP**

A, Kymographs of different constructs used in Fig. 2, in 2 mM ATP and BRB80. **B**, Kymographs of different constructs used in Fig. 2, in 2 mM ADP and BRB80.

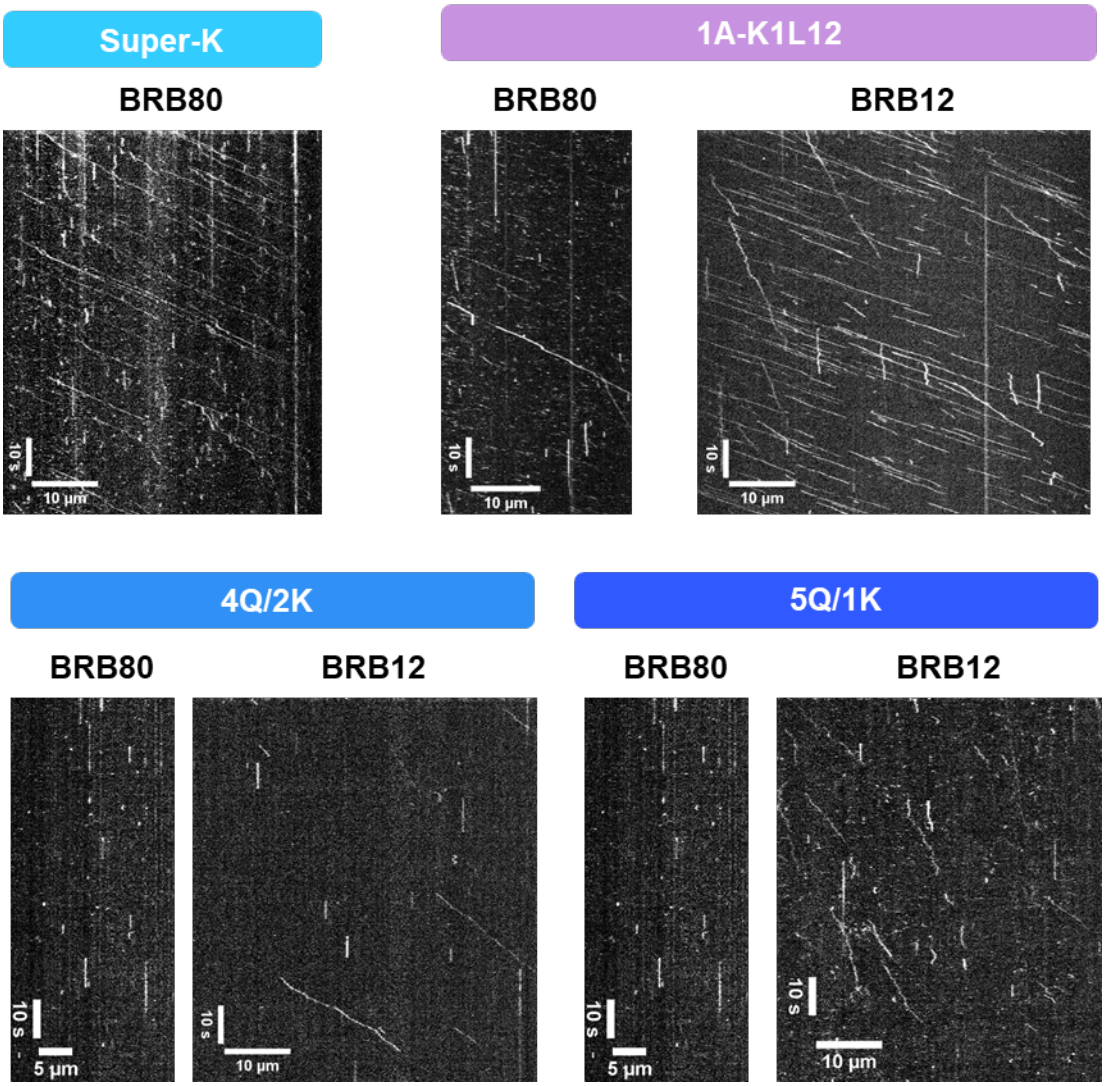

Figure S4: **Example Kymographs of Charge Mutants in BRB80 and BRB12**

Representative kymographs for the data presented in Figure 4.

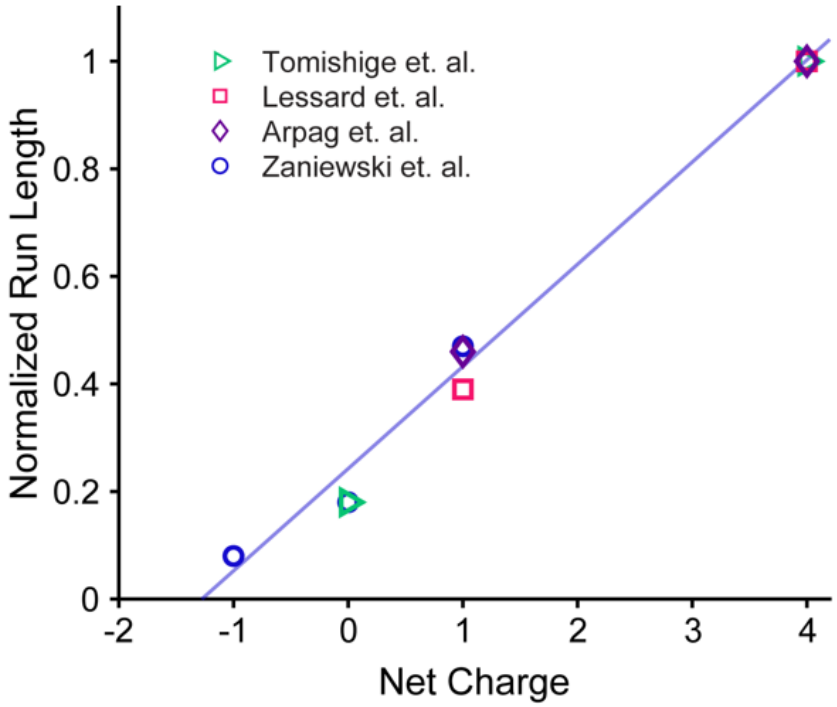

	Construct	K-Loop Charge	RL (μm)	RL (norm)
Tomishige *et. al.* [30]	Unc104-WT	4	9.5	1
	Unc104-Swap	0	1.8	0.2
Lessard *et. al.* [27]	1A-WT-LZ	4	6.2	1
	1A-3Ala-LZ	1	2.4	0.4
Arpag *et. al.* [19]	1A-WT-LZ	4	7.9	1
	1A-Swap-LZ	1	3.6	0.5
Zaniewski *et. al.* *(this study)*	$1A_{393}$	4	14.3	1
	1AK1L12	1	6.7	0.5
	1A-4Q	0	2.6	0.2
	1A-5Q	-1	1.2	0.1

Figure S5: **Published run lengths versus K-loop charge for stably dimerized KIF1A constructs in BRB12**

(Top) Plot of normalized run length versus net charge of Loop-12 for the present study and three published studies. Run lengths are normalized to the respective wild-type value (+4 net charge) for each study. Line represents fit to the relative run length versus charge for the present study (see Figure 5 for plot of non-normalized data). All experiments were performed in 12 mM PIPES buffer using constitutively active KIF1A dimers stabilized by an added coiled-coil domain. (Bottom) Actual and normalized run lengths from the four studies.